Nucleon distribution amplitudes and proton decay matrix elements on the lattice

Vladimir M. Braun,[1] Meinulf Göckeler,[1] Roger Horsley,[2] Thomas Kaltenbrunner,[1] Yoshifumi Nakamura,[3] Dirk Pleiter,[3] Paul E. L. Rakow,[4] Andreas Schäfer,[1,5] Gerrit Schierholz,[1,3] Hinnerk Stüben,[6] Nikolaus Warkentin,[1] and James M. Zanotti[2]

(QCDSF Collaboration)

[1]*Institut für Theoretische Physik, Universität Regensburg, 93040 Regensburg, Germany*
[2]*School of Physics and Astronomy, University of Edinburgh, Edinburgh EH9 3JZ, United Kingdom*
[3]*Deutsches Elektronen-Synchrotron DESY and John von Neumann Institut für Computing NIC, 15738 Zeuthen, Germany*
[4]*Theoretical Physics Division, Department of Mathematical Sciences, University of Liverpool, Liverpool L69 3BX, United Kingdom*
[5]*Yukawa Institute for Theoretical Physics, Kyoto University, Japan*
[6]*Konrad-Zuse-Zentrum für Informationstechnik Berlin, 14195 Berlin, Germany*

(Received 3 December 2008; published 13 February 2009)

Baryon distribution amplitudes (DAs) are crucial for the theory of hard exclusive reactions. We present a calculation of the first few moments of the leading-twist nucleon DA within lattice QCD. In addition we deal with the normalization of the next-to-leading (twist-four) DAs. The matrix elements determining the latter quantities are also responsible for proton decay in grand unified theories. Our lattice evaluation makes use of gauge field configurations generated with two flavors of clover fermions. The relevant operators are renormalized nonperturbatively with the final results given in the $\overline{\text{MS}}$ scheme. We find that the deviation of the leading-twist nucleon DA from its asymptotic form is less pronounced than sometimes claimed in the literature.

DOI: 10.1103/PhysRevD.79.034504 PACS numbers: 12.38.Gc, 11.15.Ha

I. INTRODUCTION

The notion of baryon distribution amplitudes (DAs) refers to the valence component of the Bethe-Salpeter wave function at small transverse separations and is central for the theory of hard exclusive reactions involving baryons [1–9]. As usual for a field theory, extraction of the asymptotic behavior (in our case for vanishing transverse separation) introduces divergences that can be studied by the renormalization-group (RG) method. The distribution amplitude φ thus becomes a function of the three quark momentum fractions x_i and the scale that serves as a UV cutoff in the allowed transverse momenta. Solving the corresponding RG equations in leading logarithmic accuracy [10,11] one is led to the expansion

$$\varphi(x_i, \mu^2) = 120 x_1 x_2 x_3 \sum_{n=0}^{\infty} \sum_{l=0}^{n} c_{nl}(\mu_0) P_{nl}(x_i) \times \left(\frac{\alpha_s(\mu)}{\alpha_s(\mu_0)}\right)^{\gamma_{nl}/\beta_0}. \quad (1)$$

The summation goes over all multiplicatively renormalizable operators built of three quarks and n derivatives and β_0 is the first coefficient of the beta function. The polynomials $P_{nl}(x_i)$ and anomalous dimensions γ_{nl} are obtained by diagonalizing the mixing matrix for the three-quark operators

$$(D_+^{k_1} q)(D_+^{k_2} q)(D_+^{k_3} q), \qquad k_1 + k_2 + k_3 = n,$$

and the $c_{nl}(\mu_0)$ are the corresponding (nonperturbative) matrix elements.

The theory of nucleon DAs has reached a certain degree of maturity. In particular the scale dependence is well understood [12,13] and it reveals important symmetries of the quantum theory that are not seen at the level of the QCD Lagrangian [14]. At the same time, they are much less studied as compared to the usual parton distributions. One reason is that the approach to the perturbative factorization regime in hard reactions appears to be slow. There is overwhelming evidence that, e.g., electromagnetic and transition form factors at currently available momentum transfers of the order of a few GeV^2 [15–18] receive large nonfactorizable contributions from large transverse distances, usually referred to as soft (Feynman) or end point contributions, and possibly from higher-twist corrections. This is indicated, for example, by the fact that the helicity selection rules are strongly violated. Another reason is that nucleon DAs enter physical observables in a rather complicated way through convolution integrals, integrated with smooth functions of the momentum fractions. This makes an experimental determination of the DAs pointwise in x_i very difficult. A qualitative picture suggested by QCD sum rule calculations is that the valence quark with the spin parallel to that of the proton carries most of its momentum [8,9,19]. It is timely to make this picture quantitative; lattice QCD ist best suited for this purpose [20–22], allowing us to evaluate nonperturbative hadronic matrix ele-

ments of local operators that enter the expansion in (1) in a fully controllable fashion, at least in principle.

In this work we report on the calculation of the first few moments of the leading-twist nucleon DA and also the normalization of the next-to-leading (twist-four) DAs [23] using two dynamical flavors of clover fermions. The reason why we also consider higher-twist DAs is that they enter the calculation of the helicity-violating Pauli form factor of the nucleon in perturbative QCD [24] and also the calculation of the soft (end point) corrections to the form factors in the framework of the light-cone sum rule approach [25,26]. Their knowledge is imperative for a QCD description of exclusive reactions in the JLAB energy range. It turns out that the same matrix elements are responsible for proton decay in grand unified theories (GUTs), so they are also interesting in a broader physics context. A short presentation of our main results has already been given in Refs. [27,28].

The paper is organized as follows. Section II contains a brief review of the general framework and definitions of the specific quantities that will be calculated. We focus on the relations to local matrix elements including those that are relevant for proton decay.

In Sec. III we explain the lattice approach to the calculation of the matrix elements. The advantages of this method come at the cost of reduced symmetry due to the discretization of space-time. This leads to additional (unwanted) operator mixing as compared to the continuum, which has to be reduced as much as possible by a suitable choice of the operator basis. In particular, mixing with lower-dimensional operators is dangerous. The theoretical basis for the corresponding analysis is the classification of operators according to irreducible representations of the relevant lattice symmetry group. For quark-antiquark operators such a classification has been worked out in Ref. [29], while the analogous classification for the three-quark operators needed here is treated in Refs. [30,31].

Section IV is devoted to the presentation of the numerical results for the matrix elements. We apply two different methods to analyze the data. The first one, which we refer to as unconstrained, is used to determine the normalization constants and to check the consistency of our results for higher moments. In the second method we use the momentum conservation as an additional constraint. This allows us to improve the accuracy of our results for the higher moments.

In Sec. V we construct a model for the leading-twist DA, presenting our results in form of the canonical expansion Eq. (1), and compare it with other models in the literature. The final Sec. VI is reserved for a summary and conclusions.

Some further technical details are presented in the Appendices, in particular, the relations between the local operators relevant for leading-twist DAs of spin-1/2 baryons and the irreducible three-quark operators. We also present here the bare lattice results.

II. GENERAL FRAMEWORK

A. Leading twist

The leading-twist proton DA can be defined [32,33] from a matrix element of a gauge-invariant nonlocal three-quark operator:

$$\begin{aligned}\langle 0|u_\alpha^{a'}(z_1)u_\beta^{b'}(z_2)d_\gamma^{c'}(z_3)U_{a'a}(z_1,z_0)U_{b'b}(z_2,z_0)&\\ \times U_{b'b}(z_3,z_0)\epsilon^{abc}|p\rangle&\\ =\frac{f_N}{4}\{(\not{p}C)_{\alpha\beta}(\gamma_5 N)_\gamma V(z_i p)+(\not{p}\gamma_5 C)_{\alpha\beta}N_\gamma A(z_i p)&\\ +(i\sigma_{\mu\nu}p^\nu C)_{\alpha\beta}(\gamma_\mu\gamma_5 N)_\gamma T(z_i p)\}+\ldots&\end{aligned} \tag{2}$$

Here $\sigma_{\mu\nu}=\frac{i}{2}[\gamma_\mu,\gamma_\nu]$, C is the charge conjugation matrix, $|p\rangle$ is a proton state with momentum p, and N is the proton spinor; ellipses stand for the higher-twist contributions. All interquark separations are assumed to be lightlike, e.g., $u(z_1)$ denotes the u-quark field at the space point $z_1 n$ with $n^2=0$, and $U(z_n,z_0)$ denotes the non-Abelian phase factor (lightlike Wilson line)

$$U(z_n,z_0)\equiv \mathrm{Pexp}\left[ig\int_0^1 dt(z_n-z_0)n_\mu A^\mu(tz_n+(1-t)z_0)\right]. \tag{3}$$

Because of the light-cone kinematics, the matrix element does not depend on z_0 and the phase factors can be eliminated by choosing a suitable gauge.

The invariant functions V, A, and T can be presented in the form

$$V(z_i p)\equiv\int[dx]\exp\left[-i\sum x_i z_i(p\cdot n)\right]V(x_i), \tag{4}$$

and similarly for A and T, where the integration measure is defined as

$$\int[dx]\equiv\int_0^1 dx_1dx_2dx_3\,\delta(1-x_1-x_2-x_3). \tag{5}$$

The variables x_i have the meaning of the longitudinal momentum fractions carried by the three quarks in the proton, $0\le x_i\le 1$ and $\sum x_i=1$.

The identity of the two u-quarks in (2) implies the following symmetry properties [33]

$$\begin{aligned}V(x_1,x_2,x_3)&=V(x_2,x_1,x_3),\\ A(x_1,x_2,x_3)&=-A(x_2,x_1,x_3),\\ T(x_1,x_2,x_3)&=T(x_2,x_1,x_3).\end{aligned} \tag{6}$$

In addition, the requirement that the proton has isospin 1/2 yields the relation

$$2T(x_1,x_2,x_3)=[V-A](x_1,x_3,x_2)-[V-A](x_2,x_3,x_1) \tag{7}$$

so that all three invariant functions can be expressed in terms of a single DA φ defined as

$$\varphi(x_1, x_2, x_3) = V(x_1, x_2, x_3) - A(x_1, x_2, x_3). \quad (8)$$

The normalization convention is such that

$$\int [dx]\varphi(x_1, x_2, x_3) = 1. \quad (9)$$

The definition in (2) is equivalent to the following form of the proton state [9,33]

$$|p, \uparrow\rangle = f_N \int \frac{[dx]\varphi(x_i)}{2\sqrt{24 x_1 x_2 x_3}} \{|u^\uparrow(x_1)u^\downarrow(x_2)d^\uparrow(x_3)\rangle - |u^\uparrow(x_1)d^\downarrow(x_2)u^\uparrow(x_3)\rangle\}, \quad (10)$$

where the arrows indicate the helicities and the standard relativistic normalization for the states and Dirac spinors is implied.

Moments of DAs are defined as

$$V^{lmn} = \int_0^1 [\mathrm{d}x] x_1^l x_2^m x_3^n V(x_1, x_2, x_3) \quad (11)$$

and similarly for the other functions. They can be related to matrix elements of the local operators

$$\begin{aligned}\mathcal{V}_\tau^{\rho \bar{l}\bar{m}\bar{n}}(0) &\equiv \mathcal{V}_\tau^{\rho(\lambda_1\cdots\lambda_l)(\mu_1\cdots\mu_m)(\nu_1\cdots\nu_n)}(0) \\ &= \epsilon^{abc}[i^l D^{\lambda_1}\ldots D^{\lambda_l}u(0)]_\alpha^a (C\gamma^\rho)_{\alpha\beta} \\ &\quad \times [i^m D^{\mu_1}\ldots D^{\mu_m}u(0)]_\beta^b \\ &\quad \times [i^n D^{\nu_1}\ldots D^{\nu_n}(\gamma_5 d(0))]_\tau^c, \end{aligned} \quad (12)$$

$$\begin{aligned}\mathcal{A}_\tau^{\rho \bar{l}\bar{m}\bar{n}}(0) &\equiv \mathcal{A}_\tau^{\rho(\lambda_1\cdots\lambda_l)(\mu_1\cdots\mu_m)(\nu_1\cdots\nu_n)}(0) \\ &= \epsilon^{abc}[(i^l D^{\lambda_1}\ldots D^{\lambda_l}u(0)]_\alpha^a (C\gamma^\rho\gamma_5)_{\alpha\beta} \\ &\quad \times [i^m D^{\mu_1}\ldots D^{\mu_m}u(0)]_\beta^b \\ &\quad \times [i^n D^{\nu_1}\ldots D^{\nu_n}d(0)]_\tau^c, \end{aligned} \quad (13)$$

$$\begin{aligned}\mathcal{T}_\tau^{\rho \bar{l}\bar{m}\bar{n}}(0) &\equiv \mathcal{T}_\tau^{\rho(\lambda_1\cdots\lambda_l)(\mu_1\cdots\mu_m)(\nu_1\cdots\nu_n)}(0) \\ &= \epsilon^{abc}[i^l D^{\lambda_1}\ldots D^{\lambda_l}u(0)]_\alpha^a (C(-i\sigma^{\xi\rho}))_{\alpha\beta} \\ &\quad \times [i^m D^{\mu_1}\ldots D^{\mu_m}u(0)]_\beta^b \\ &\quad \times [i^n D^{\nu_1}\ldots D^{\nu_n}(\gamma_\xi\gamma_5 d(0))]_\tau^c \end{aligned} \quad (14)$$

by

$$P_{LTW}\langle 0|\mathcal{V}_\tau^{\rho \bar{l}\bar{m}\bar{n}}(0)|p\rangle = -f_N V^{lmn} p^\rho p^{\bar{l}} p^{\bar{m}} p^{\bar{n}} N_\tau(p), \quad (15)$$

$$P_{LTW}\langle 0|\mathcal{A}_\tau^{\rho \bar{l}\bar{m}\bar{n}}(0)|p\rangle = -f_N A^{lmn} p^\rho p^{\bar{l}} p^{\bar{m}} p^{\bar{n}} N_\tau(p), \quad (16)$$

$$P_{LTW}\langle 0|\mathcal{T}_\tau^{\rho \bar{l}\bar{m}\bar{n}}(0)|p\rangle = 2 f_N T^{lmn} p^\rho p^{\bar{l}} p^{\bar{m}} p^{\bar{n}} N_\tau(p). \quad (17)$$

In the following we refer to these local operators as DA operators in order to distinguish them from three-quark operators with a general spinor index structure. The multi-index $\bar{l}\,\bar{m}\,\bar{n}$ with $\bar{l} \equiv \lambda_1 \ldots \lambda_l$ (and similarly for $\bar{m}$ and $\bar{n}$) denotes the Lorentz structure given by the covariant derivatives $D_\mu = \partial_\mu - igA_\mu$ on the right-hand side of Eqs. (12)–(14). The indices l, m, n (without bars) are the total number of derivatives acting on the first, second, and third quark, respectively. A certain moment, e.g., V^{lmn}, is related to several operators $V_\tau^{\rho \bar{l}\bar{m}\bar{n}}$ which differ only by their Lorentz indices. Therefore the moments V^{lmn}, A^{lmn}, and T^{lmn} on the right-hand side of Eqs. (15)–(17) can be calculated from different operators with same number of derivatives acting on the quark fields. The index ρ corresponds to the uncontracted Lorentz index of the gamma matrices in the operators. The leading-twist projection, P_{LTW}, can be achieved, e.g., by symmetrization in Lorentz indices and subtraction of traces. Our approach for handling the reduced symmetry of the discretized space-time properly is described in Sec. III.

The symmetry relations (6) are translated into similar relations for the moments:

$$V^{lmn} = V^{mln}, \qquad A^{lmn} = -A^{mln}, \qquad T^{lmn} = T^{mln}. \quad (18)$$

For further use we define the combination

$$\phi^{lmn} = \frac{1}{3}(V^{lmn} - A^{lmn} + 2T^{lnm}). \quad (19)$$

Taking into account the isospin relation (7), the moments of V, A, T can be restored from the moments of ϕ by

$$T^{lmn} = \frac{1}{2}(\phi^{lnm} + \phi^{mnl}), \quad (20)$$

$$V^{lmn} = \frac{1}{2}(2\phi^{lmn} + 2\phi^{mln} - \phi^{nlm} - \phi^{nml}), \quad (21)$$

$$A^{lmn} = \frac{1}{2}(-2\phi^{lmn} + 2\phi^{mln} - \phi^{nlm} + \phi^{nml}). \quad (22)$$

The conventional proton DA $\varphi(x_i)$ (8) is given in terms of $\phi(x_i)$ as

$$\begin{aligned}\varphi(x_1, x_2, x_3) &= 2\phi(x_1, x_2, x_3) - \phi(x_3, x_2, x_1), \\ \varphi^{lmn} &= 2\phi^{lmn} - \phi^{nml}. \end{aligned} \quad (23)$$

Because of momentum conservation ($x_1 + x_2 + x_3 = 1$) there are additional relations between lower and higher moments:

$$\phi^{lmn} = \phi^{(l+1)mn} + \phi^{l(m+1)n} + \phi^{lm(n+1)}. \quad (24)$$

In particular this implies

$$\begin{aligned}1 &= \phi^{000} = \phi^{100} + \phi^{010} + \phi^{001} \\ &= \phi^{200} + \phi^{020} + \phi^{002} + 2(\phi^{011} + \phi^{101} + \phi^{110}) = \ldots \end{aligned} \quad (25)$$

B. Next-to-leading twist operators and proton decay

In general, there exist three independent next-to-leading (twist-four) three-quark DAs, cf. Ref. [23]. In this work we only consider their normalization, which is related to the contributions of local operators without derivatives. Thus the problem is simplified considerably since the general Lorentz decomposition of the relevant matrix element involves only four structures:

$$\begin{aligned}4\langle 0|\epsilon^{abc}u^a_\alpha(0)u^b_\beta(0)d^c_\gamma(0)|p\rangle &= V_1^0(\not{p}C)_{\alpha\beta}(\gamma_5 N)_\gamma + V_3^0 m_N(\gamma_\mu C)_{\alpha\beta}(\gamma^\mu\gamma_5 N)_\gamma \\ &+ T_1^0(p^\nu i\sigma_{\mu\nu}C)_{\alpha\beta}(\gamma^\mu\gamma_5 N)_\gamma \\ &+ T_3^0 m_N(\sigma_{\mu\nu}C)_{\alpha\beta}(\sigma^{\mu\nu}\gamma_5 N)_\gamma,\end{aligned} \tag{26}$$

where m_N is the nucleon mass and we have used the same notation as in [23]. The leading-twist-three constants V_1^0 and T_1^0 correspond to $f_N V^{000}$ and $f_N T^{000}$ in our notation, Eqs. (15) and (17), and are equal. The two additional constants, V_3^0 and T_3^0, correspond to subleading twist-four contributions. The combinations $\lambda_1 = V_1^0 - 4V_3^0$ and $\lambda_2 = 6(V_1^0 - 4T_3^0)$ are often arising in QCD sum rule calculations. They describe the nucleon coupling to the two independent local operators

$$\mathcal{L}_\tau(0) = \epsilon^{abc}[u^{aT}(0)C\gamma^\rho u^b(0)]\times(\gamma_5\gamma_\rho d^c(0))_\tau, \tag{27}$$

$$\mathcal{M}_\tau(0) = \epsilon^{abc}[u^{aT}(0)C\sigma^{\mu\nu}u^b(0)]\times(\gamma_5\sigma_{\mu\nu}d^c(0))_\tau, \tag{28}$$

which have been introduced in [34,35], respectively. Their matrix elements are given by

$$\langle 0|\mathcal{L}_\tau(0)|p\rangle = \lambda_1 m_N N_\tau, \tag{29}$$

$$\langle 0|\mathcal{M}_\tau(0)|p\rangle = \lambda_2 m_N N_\tau. \tag{30}$$

Separating the components of different helicity, one can write

$$\mathcal{L}_\tau = 4(\gamma_R\mathcal{U}^L - \gamma_L\mathcal{U}^R)_\tau, \tag{31}$$

$$\mathcal{M}_\tau = 8(\gamma_R\mathcal{U}^R - \gamma_L\mathcal{U}^L)_\tau, \tag{32}$$

where $\gamma_L = (1-\gamma_5)/2$, $\gamma_R = (1+\gamma_5)/2$ are the left- and right-handed projectors and

$$\mathcal{U}^{L/R}_\tau = \epsilon^{abc}u^a_\tau[(\gamma_{L/R}u^b)^T C\gamma_{L/R}d^c]. \tag{33}$$

The Fierz identity implies

$$\begin{aligned}\epsilon^{abc}[u^{aT}(0)C\gamma^\mu u^b(0)](\gamma_5\gamma_\mu d^c(0))_\tau &= 2\epsilon^{abc}(-[u^{aT}(0)C\gamma_5 d^b(0)]u^c(0)_\tau \\ &+ [u^{aT}(0)Cd^b(0)](\gamma_5 u^c(0))_\tau),\end{aligned} \tag{34}$$

$$\begin{aligned}\epsilon^{abc}[u^{aT}(0)C\sigma^{\mu\nu}u^b(0)](\gamma_5\sigma_{\mu\nu}d^c(0))_\tau &= 4\epsilon^{abc}([u^{aT}(0)C\gamma_5 d^b(0)]u^c(0)_\tau \\ &+ [u^{aT}(0)Cd^b(0)](\gamma_5 u^c(0))_\tau).\end{aligned} \tag{35}$$

Thus we get

$$m_N(2\lambda_1+\lambda_2)N(p) = 8\langle 0|\epsilon^{abc}(u^{aT}Cd^b)\gamma_5 u^c|p\rangle, \tag{36}$$

where, as it can be shown, the matrix element on the right-hand side vanishes in the nonrelativistic limit.

The operators (27) and (28) appear also in the low-energy effective action of generic GUT models, and their matrix elements $\langle\pi|\mathcal{L}|p\rangle$ and $\langle\pi|\mathcal{M}|p\rangle$ give rise to proton decay. These matrix elements, in turn, can be related to the constants defined in (29) and (30), using soft pion theorems or, what is the same, leading order in chiral perturbation theory [36–40].

To this end one introduces two low-energy constants α and β which extend the usual three-flavor baryon chiral Lagrangian. They are defined by

$$\begin{aligned}\langle 0|(\gamma_L\mathcal{U}^R)_\tau(0)|p\rangle &= -\alpha(\gamma_L N)_\tau, \\ \langle 0|(\gamma_R\mathcal{U}^L)_\tau(0)|p\rangle &= \alpha(\gamma_R N)_\tau,\end{aligned} \tag{37}$$

$$\begin{aligned}\langle 0|(\gamma_L\mathcal{U}^L)_\tau(0)|p\rangle &= -\beta(\gamma_L N)_\tau, \\ \langle 0|(\gamma_R\mathcal{U}^R)_\tau(0)|p\rangle &= \beta(\gamma_R N)_\tau.\end{aligned} \tag{38}$$

Because of (31) and (32) one obtains $\alpha = m_N\lambda_1/4$ and $\beta = m_N\lambda_2/8$. The knowledge of these two constants allows one to estimate nucleon-to-pion decay matrix elements. Using the notation of Ref. [41] the relevant factors in the decay amplitude for the proton to π^0 decay (cf. Figure 1) have the form

$$W_0^{RL}(p\to\pi^0) = \frac{\alpha}{\sqrt{2}f}(1+g_A), \tag{39}$$

$$W_0^{LL}(p\to\pi^0) = \frac{\beta}{\sqrt{2}f}(1+g_A), \tag{40}$$

where f is the tree level pion decay constant normalized such that the experimental value is $f_\pi \simeq 131$ MeV and g_A is the axial charge.

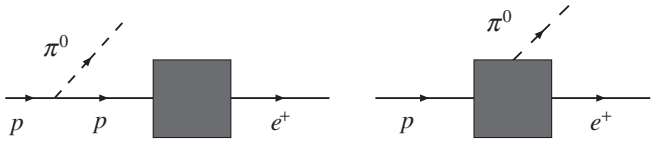

FIG. 1. Diagrams contributing to the nucleon decay amplitude $p\to\pi^0+e^+$.

III. DETAILS OF THE LATTICE CALCULATION

In this section we discuss the techniques used and the details of the lattice calculation. From now on we work in Euclidean space. In order to define the Euclidean counterparts of the operators Eqs. (12)–(14), (27), (28), and (33) we interpret the Dirac matrices and coordinates as being Euclidean. For our Euclidean Dirac matrices see Appendix A. The expressions on the right-hand-side of Eqs. (12)–(14), (27), and (28) are then modified accordingly. In the first part of this section we summarize the general features of our approach. The following parts contain the description of the calculation of matrix elements relevant for leading and next-to-leading twist DAs.

A. General features

To be as flexible as possible in our calculation we have adopted a two-stage approach in the evaluation of the correlators. In the first step we have calculated correlators of the form

$$C^{\bar{l}\bar{m}\bar{n}}_{\alpha\beta\gamma\tau} = \langle \epsilon^{abc}[D_{\lambda_1}\dots D_{\lambda_l}u(x)]^a_\alpha [D_{\mu_1}\dots D_{\mu_m}u(x)]^b_\beta \times [D_{\nu_1}\dots D_{\nu_n}d(x)]^c_\gamma \overline{\mathcal{N}}(y)_\tau\rangle, \quad (41)$$

with $l+m+n \le 2$. As interpolating operator for the proton we have used

$$\mathcal{N}_\tau = \epsilon^{abc}[u^{aT}C\gamma_5 d^b]u^c_\tau. \quad (42)$$

Because of the presence of two u-quarks in the three-quark operator, $C^{\bar{m}\bar{l}\bar{n}}_{\alpha\beta\gamma\tau}$ can be reconstructed from $C^{\bar{l}\bar{m}\bar{n}}_{\alpha\beta\gamma\tau}$ by an appropriate interchange of Dirac indices.

In the second step the general three-quark operator from Eq. (41) was used to calculate the matrix elements for the different quantities we discussed before. The general form of the correlation functions we compute at this stage reads after projection onto momentum $\vec{p}$:

$$\langle \mathcal{O}_\tau(t,\vec{p})\overline{\mathcal{N}}_{\tau'}(0,\vec{p})\rangle = \frac{\sqrt{Z_N(\vec{p})}}{2E(\vec{p})}\sum_s \langle 0|\mathcal{O}_\tau(0)|p,s\rangle \overline{N}_{\tau'}(p,s) \times \exp(-E(\vec{p})t). \quad (43)$$

Here contributions of excited states have been neglected and the dependence of the nucleon states and spinors on the spin vector s has been made explicit. For the energy $E(\vec{p})$ we use the continuum expression $E(\vec{p}) = \sqrt{m_N^2 + \vec{p}^2}$. We have checked that this dispersion relation is fulfilled well within errors (see, e.g., Fig. 2), so we had to fit only the mass in the exponential. The correlator in Eq. (43) can be directly constructed from the general correlation function (41). The matrix element on the right-hand side is the quantity we want to determine. Thus we have also to calculate the normalization constant $Z_N(\vec{p})$, which can be extracted from the usual two-point nucleon correlator

$$C_N(\vec{p}) \equiv (\gamma_+)_{\tau'\tau}\langle \mathcal{N}_\tau(t,\vec{p})\overline{\mathcal{N}}_{\tau'}(0,\vec{p})\rangle = Z_N(\vec{p})\frac{m_N + E(\vec{p})}{E(\vec{p})}\exp(-E(\vec{p})t) \quad (44)$$

with the positive parity projection $\gamma_+ = (1+\gamma_4)/2$. In the evaluation of the correlator in Eq. (41) the overlap of the nucleon interpolator with the nucleon state is improved by Jacobi smearing at the source while the sink is not smeared since we want to evaluate local matrix elements. Thus the nucleon correlator in Eq. (44) cannot be extracted from the general three-quark nucleon correlator (41) but must be computed separately with Jacobi smeared sink and source.

The normalization constant $Z_N(\vec{p})$ could be removed by considering the ratio

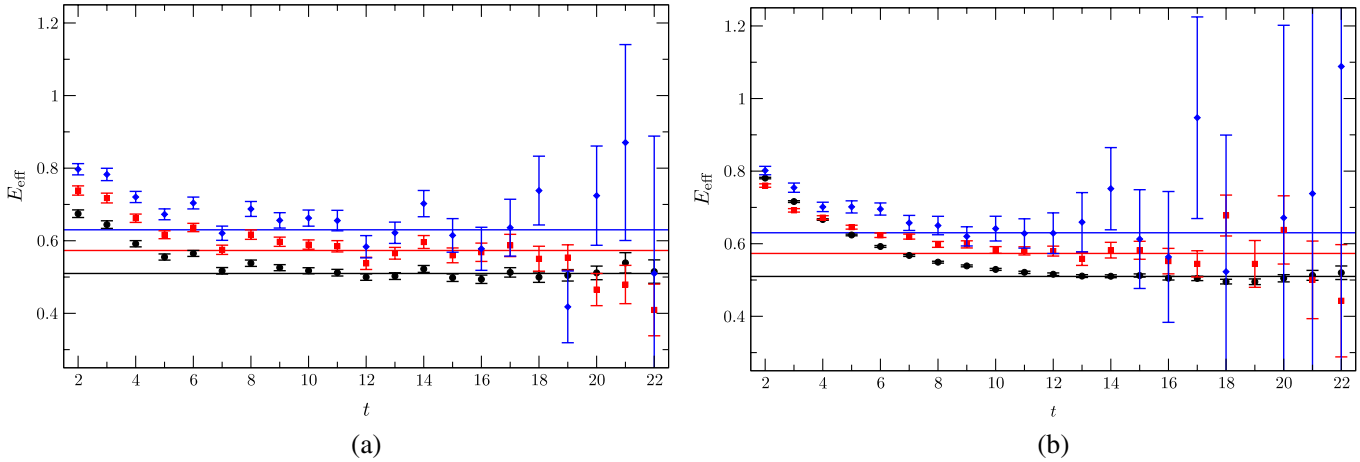

FIG. 2 (color online). Effective energy plots for different nucleon momenta at $\beta = 5.40$ and $\kappa = 0.13610$ for the nucleon correlator (a) and the distribution amplitude correlators (b), where we have averaged over all available correlators. The black circles were obtained at zero nucleon momentum, the red squares and blue diamonds correspond to $\vec{p}^2 = (2\pi/L)^2$ and $\vec{p}^2 = 2(2\pi/L)^2$, respectively. The lowest black line shows the nucleon mass as obtained by direct calculation. The middle red and the top blue line correspond to energies $E^2_{\rm eff} = m^2_{\rm eff} + \vec{p}^2$ with $\vec{p}^2 = (2\pi/L)^2$ and $\vec{p}^2 = 2(2\pi/L)^2$, respectively.

$$\frac{((\gamma_+)_{\tau'\tau}\langle \mathcal{O}_\tau(t)\overline{\mathcal{N}}_{\tau'}(0)\rangle)^2}{(\gamma_+)_{\tau'\tau}\langle \mathcal{N}_\tau(t)\overline{\mathcal{N}}_{\tau'}(0)\rangle}. \tag{45}$$

However, as we will see later, the location of the effective mass plateaus is different for the two correlators, presumably due to the different smearings on the sink, spoiling this simple approach. Thus instead of calculating the ratio we perform a correlated fit to the two correlators in the range of the corresponding effective mass plateaus.

Up to now we did not take into account that our calculations are performed on a space-time lattice. This leads to reduced symmetry compared to the continuum. Because of this symmetry reduction we expect additional operator mixings which are not present in the continuum. In particular, we can have mixing with lower-dimensional operators. Thus a systematic analysis and careful choice of the operators used is mandatory. In [31] a complete classification with respect to the spinorial extension of the hypercubic group $H(4)$ for all three-quark operators without derivatives is presented. For operators with one and two derivatives the classification is worked out for the leading-twist case. These results enable us to derive operators with ''good'' mixing properties, good in the sense that they do not mix with lower-dimensional operators. They belong to definite irreducible representations of the spinorial extension of $H(4)$ and are most easily constructed in the Weyl representation of the Dirac matrices. Therefore we also work in this representation.

In Table I we give an overview of the irreducible multiplets of operators taken from Table 4.1 in [31], with a modified notation adapted to our needs, e.g., operator $B^{(2)}_{1,i}$ corresponds to $\mathcal{O}^{(i)}_{DD1}$ in [31] and similarly for the others. The next-to-leading twist operators (27) and (28) lie completely within the τ_1^4 representation with mass dimension $9/2$. The operators relevant for the leading-twist DAs belong to other multiplets. As operators without derivatives in the $\tau^{\underline{8}}$ representation do not have an overlap with the nucleon, the relevant operators with good mixing properties lie in τ_1^{12}, τ_2^{12}, and τ_2^4 for zero, one and two derivatives, respectively. Rewriting these irreducible operators in terms of the DA operators defined in (12)–(14) allows us to choose those that are suited for lattice calculations. The ensuing relations for leading-twist spin-$1/2$ baryon DAs are summarized in Appendix B. In the following we give some details for these operators.

Initially, the irreducible operators in [31] have a general flavor content. Considering the case of two derivatives as an example we have operators of the type

$$\Gamma^{\alpha\beta\gamma}_{\mu\nu} D_\mu D_\nu \epsilon^{abc} f^a_\alpha g^b_\beta h^c_\gamma, \tag{46}$$

where $\Gamma^{\alpha\beta\gamma}_{\mu\nu}$ is a tensor projecting the operator to a certain irreducible representation. As it is not important for the construction of irreducibly transforming operators on which of the quarks the derivatives act, the different possibilities fall into the same irreducible representation. The proton operators are then recovered by the identification

$$f \to u, \qquad g \to u, \qquad h \to d, \tag{47}$$

and subsequent projection onto isospin $1/2$, which is done by combining properly different multiplets. This procedure differs somewhat from the approach adopted in Ref. [31], but it leads to equivalent results.

The operators used in our calculation have to be renormalized. In [42,43] the required renormalization matrices were calculated nonperturbatively on the lattice imposing an RI′-MOM-like renormalization condition. Using continuum perturbation theory and the renormalization group the results were converted to the $\overline{\text{MS}}$ scheme at a scale of 4 GeV^2. Note that in this procedure the mixing with ''total derivatives'' is automatically taken into account. The scale at which our renormalization condition is imposed is taken to be 20 GeV^2, and the systematic uncertainty is estimated by varying this scale between 10 GeV^2 and 40 GeV^2.

B. Moments of the leading-twist DA

1. 0th moment

Using the representation τ_1^{12} and the relations to the DA operators given in Appendix B we construct three quad-

TABLE I. Overview of irreducibly transforming multiplets of three-quark operators sorted by their mass dimension (number of derivatives) taken from [31] with a notation adapted to our needs. Since for the classification it is not important on which quarks the derivatives act, only the sum $l + m + n$ is given as a superscript. The subscript gives the numbering of the operators according to the numbering convention in [31]. The first number corresponds to the lower index of [31] while the second number corresponds to the upper index in [31] labelling different operators within one multiplet (cf. Table 4.1 in [31]). In the first column we give also the representations in the notation of [31] where the superscript denotes the dimension.

	$d = 9/2$ (0 derivatives)	$d = 11/2$ (1 derivative)	$d = 13/2$ (2 derivatives)
τ_1^4	$\mathcal{B}^{(0)}_{1,i}$, $\mathcal{B}^{(0)}_{2,i}$, $\mathcal{B}^{(0)}_{3,i}$, $\mathcal{B}^{(0)}_{4,i}$, $\mathcal{B}^{(0)}_{5,i}$		$\mathcal{B}^{(2)}_{1,i}$, $\mathcal{B}^{(2)}_{2,i}$, $\mathcal{B}^{(2)}_{3,i}$
τ_2^4			$\mathcal{B}^{(2)}_{4,i}$, $\mathcal{B}^{(2)}_{5,i}$, $\mathcal{B}^{(2)}_{6,i}$
$\tau^{\underline{8}}$	$\mathcal{B}^{(0)}_{6,i}$	$\mathcal{B}^{(1)}_{1,i}$	$\mathcal{B}^{(2)}_{7,i}$, $\mathcal{B}^{(2)}_{8,i}$, $\mathcal{B}^{(2)}_{9,i}$
τ_1^{12}	$\mathcal{B}^{(0)}_{7,i}$, $\mathcal{B}^{(0)}_{8,i}$, $\mathcal{B}^{(0)}_{9,i}$	$\mathcal{B}^{(1)}_{2,i}$, $\mathcal{B}^{(1)}_{3,i}$, $\mathcal{B}^{(1)}_{4,i}$	$\mathcal{B}^{(2)}_{10,i}$, $\mathcal{B}^{(2)}_{11,i}$, $\mathcal{B}^{(2)}_{12,i}$, $\mathcal{B}^{(2)}_{13,i}$
τ_2^{12}		$\mathcal{B}^{(1)}_{5,i}$, $\mathcal{B}^{(1)}_{6,i}$, $\mathcal{B}^{(1)}_{7,i}$, $\mathcal{B}^{(1)}_{8,i}$	$\mathcal{B}^{(2)}_{14,i}$, $\mathcal{B}^{(2)}_{15,i}$, $\mathcal{B}^{(2)}_{16,i}$, $\mathcal{B}^{(2)}_{17,i}$, $\mathcal{B}^{(2)}_{18,i}$

ruplets of operators with isospin 1/2 from the 12 irreducible three-quark operators, which can be used to calculate f_N:

$$\mathcal{O}^{000}_{A,0} = \frac{4}{3}\begin{pmatrix} -\mathcal{B}^{000}_{8,6} & + & \mathcal{B}^{000}_{9,6} \\ \mathcal{B}^{000}_{8,1} & - & \mathcal{B}^{000}_{9,1} \\ -\mathcal{B}^{000}_{8,12} & + & \mathcal{B}^{000}_{9,12} \\ \mathcal{B}^{000}_{8,7} & - & \mathcal{B}^{000}_{9,7} \end{pmatrix},$$

$$\mathcal{O}^{000}_{B,0} = \frac{4}{3}\begin{pmatrix} -\mathcal{B}^{000}_{8,4} & + & \mathcal{B}^{000}_{9,4} \\ \mathcal{B}^{000}_{8,3} & - & \mathcal{B}^{000}_{9,3} \\ -\mathcal{B}^{000}_{8,10} & + & \mathcal{B}^{000}_{9,10} \\ \mathcal{B}^{000}_{8,9} & - & \mathcal{B}^{000}_{9,9} \end{pmatrix}, \tag{48}$$

$$\mathcal{O}^{000}_{C,0} = \frac{4\sqrt{2}}{3}\begin{pmatrix} \mathcal{B}^{000}_{8,2} & - & \mathcal{B}^{000}_{9,2} \\ -\mathcal{B}^{000}_{8,5} & + & \mathcal{B}^{000}_{9,5} \\ \mathcal{B}^{000}_{8,8} & - & \mathcal{B}^{000}_{9,8} \\ -\mathcal{B}^{000}_{8,11} & + & \mathcal{B}^{000}_{9,11} \end{pmatrix}.$$

The three-quark operators $\mathcal{O}$ on the left-hand side have also a Dirac index which we do not give explicitly here. The relations to the DA operators given in Appendix B yield then

$$\langle 0|\mathcal{O}^{000}_{A,0}|p\rangle = f_N(ip_1\gamma_1 - ip_2\gamma_2)N(p), \tag{49}$$

$$\langle 0|\mathcal{O}^{000}_{B,0}|p\rangle = f_N(ip_3\gamma_3 + E(\vec{p})\gamma_4)N(p), \tag{50}$$

$$\langle 0|\mathcal{O}^{000}_{C,0}|p\rangle = f_N(ip_1\gamma_1 + ip_2\gamma_2 - ip_3\gamma_3 + E(\vec{p})\gamma_4)N(p). \tag{51}$$

The operators $\mathcal{O}^{000}_{B,0}$ and $\mathcal{O}^{000}_{C,0}$ are most suitable for our calculation since $\mathcal{O}^{000}_{A,0}$ would require nonzero spatial momenta in the 1 or 2 direction, which would increase the statistical noise. Thus, in order to determine f_N, we evaluate finally only the following two correlators at $\vec{p} = \vec{0}$:

$$C^{000}_{B,0} \equiv \langle(\gamma_4\mathcal{O}^{000}_{B,0}(t,\vec{p}))_\tau(\overline{\mathcal{N}}(0,\vec{p}))_{\tau'}(\gamma_+)_{\tau'\tau}\rangle = f_N\sqrt{Z_N(\vec{p})}\,\frac{E(\vec{p})(m_N + E(\vec{p})) + p_3^2}{E(\vec{p})}\exp(-E(\vec{p})t), \tag{52}$$

$$C^{000}_{C,0} \equiv \langle(\gamma_4\mathcal{O}^{000}_{C,0}(t,\vec{p}))_\tau(\overline{\mathcal{N}}(0,\vec{p}))_{\tau'}(\gamma_+)_{\tau'\tau}\rangle = f_N\sqrt{Z_N(\vec{p})}\,\frac{E(\vec{p})(m_N + E(\vec{p})) + p_1^2 + p_2^2 - p_3^2}{E(\vec{p})} \times \exp(-E(\vec{p})t). \tag{53}$$

2. 1st moments

We use the irreducible operators with one derivative from Appendix B to construct operators for the calculation of the first moments of the proton DA,

$$\mathcal{O}^{lmn}_{A,1} = \frac{4\sqrt{2}}{3}\begin{pmatrix} \mathcal{B}^{lmn}_{6,1} & - & \mathcal{B}^{lnm}_{7,1} \\ -\mathcal{B}^{lmn}_{6,2} & + & \mathcal{B}^{lnm}_{7,2} \\ -\mathcal{B}^{lmn}_{6,7} & + & \mathcal{B}^{lnm}_{7,7} \\ \mathcal{B}^{lmn}_{6,8} & - & \mathcal{B}^{lnm}_{7,8} \end{pmatrix},$$

$$\mathcal{O}^{lmn}_{B,1} = \frac{4\sqrt{2}}{3}\begin{pmatrix} \mathcal{B}^{lmn}_{6,3} & - & \mathcal{B}^{lnm}_{7,3} \\ -\mathcal{B}^{lmn}_{6,4} & + & \mathcal{B}^{lnm}_{7,4} \\ -\mathcal{B}^{lmn}_{6,9} & + & \mathcal{B}^{lnm}_{7,9} \\ \mathcal{B}^{lmn}_{6,10} & - & \mathcal{B}^{lnm}_{7,10} \end{pmatrix}, \tag{54}$$

$$\mathcal{O}^{lmn}_{C,1} = \frac{4}{3}\begin{pmatrix} \mathcal{B}^{lmn}_{6,6} & - & \mathcal{B}^{lnm}_{7,6} \\ \mathcal{B}^{lmn}_{6,5} & - & \mathcal{B}^{lnm}_{7,5} \\ -\mathcal{B}^{lmn}_{6,12} & + & \mathcal{B}^{lnm}_{7,12} \\ -\mathcal{B}^{lmn}_{6,11} & + & \mathcal{B}^{lnm}_{7,11} \end{pmatrix},$$

where the superscript lmn with $l + m + n = 1$ and nonnegative integers l, m, n indicates on which fields the derivative acts. The matrix elements of these operators are then

$$\langle 0|\mathcal{O}^{lmn}_{A,1}|p\rangle = f_N\phi^{lmn}[(p_1\gamma_1 - p_2\gamma_2)(ip_3\gamma_3 - E(\vec{p})\gamma_4) - 2ip_1p_2\gamma_1\gamma_2]N(p), \tag{55}$$

$$\langle 0|\mathcal{O}^{lmn}_{B,1}|p\rangle = f_N\phi^{lmn}[(p_1\gamma_1 + p_2\gamma_2)(ip_3\gamma_3 + E(\vec{p})\gamma_4) - 2p_3E(\vec{p})\gamma_3\gamma_4]N(p), \tag{56}$$

$$\langle 0|\mathcal{O}^{lmn}_{C,1}|p\rangle = f_N\phi^{lmn}(-p_1\gamma_1 + p_2\gamma_2)(ip_3\gamma_3 + E(\vec{p})\gamma_4)N(p), \tag{57}$$

where again a Dirac index is implied for the three-quark operators $\mathcal{O}$. Unlike the case of the 0th moment all operators require at least one nonzero component of the spatial momentum. Hence using all operators available in this case we evaluate the correlators

$$C^{lmn}_{A,1} \equiv \langle(\gamma_4\gamma_1\mathcal{O}^{lmn}_{A,1}(t,\vec{p}))_\tau(\overline{\mathcal{N}}(0,\vec{p}))_{\tau'}(\gamma_+)_{\tau'\tau}\rangle = -f_N\phi^{lmn}\sqrt{Z_N(\vec{p})}\,p_1\frac{E(\vec{p})(m_N + E(\vec{p})) + 2p_2^2 - p_3^2}{E(\vec{p})} \times \exp(-E(\vec{p})t), \tag{58}$$

$$C^{lmn}_{B,1} \equiv \langle(\gamma_4\gamma_1\mathcal{O}^{lmn}_{B,1}(t,\vec{p}))_\tau(\overline{\mathcal{N}}(0,\vec{p}))_{\tau'}(\gamma_+)_{\tau'\tau}\rangle = f_N\phi^{lmn}\sqrt{Z_N(\vec{p})}\,p_1\frac{E(\vec{p})(m_N + E(\vec{p})) + p_3^2}{E(\vec{p})} \times \exp(-E(\vec{p})t), \tag{59}$$

$$C^{lmn}_{C,1} \equiv \langle(\gamma_4\gamma_1\mathcal{O}^{lmn}_{C,1}(t,\vec{p}))_\tau(\overline{\mathcal{N}}(0,\vec{p}))_{\tau'}(\gamma_+)_{\tau'\tau}\rangle = -f_N\phi^{lmn}\sqrt{Z_N(\vec{p})}\,p_1\frac{E(\vec{p})(m_N + E(\vec{p})) + p_3^2}{E(\vec{p})} \times \exp(-E(\vec{p})t) \tag{60}$$

to determine the first moments ϕ^{100}, ϕ^{010}, and ϕ^{001}.

3. 2nd moments

The calculation of the second moments requires the use of the four-dimensional irreducible representation τ_2^4 to avoid mixing with lower-dimensional operators. Unfortunately, this decreases also the number of possible operators. Using the irreducible three-quark operators with two derivatives and the relations to the DA operators from Appendix B we construct

$$\mathcal{O}_2^{lmn} := \frac{4}{3\sqrt{3}} \begin{pmatrix} \mathcal{B}_{6,4}^{lnm} - \mathcal{B}_{5,4}^{lmn} \\ \mathcal{B}_{6,3}^{lnm} - \mathcal{B}_{5,3}^{lmn} \\ \mathcal{B}_{6,2}^{lnm} - \mathcal{B}_{5,2}^{lmn} \\ \mathcal{B}_{6,1}^{lnm} - \mathcal{B}_{5,1}^{lmn} \end{pmatrix}, \tag{61}$$

where now $l + m + n = 2$ with l, m, and n nonnegative integers. The corresponding matrix element is given by

$$\begin{aligned} \langle 0|\mathcal{O}_2^{lmn}|p\rangle = f_N \phi^{lmn}[&p_1 p_2 \gamma_1\gamma_2 (i p_3 \gamma_3 + E(\vec{p})\gamma_4) \\ &+ i p_3 E(\vec{p})\gamma_3\gamma_4 (i p_1 \gamma_1 - i p_2 \gamma_2)] N(p) \end{aligned} \tag{62}$$

and the second moments are determined from

$$\begin{aligned} C_2^{lmn} &\equiv \langle ((\gamma_2\gamma_3\gamma_4 \mathcal{O}_2^{lmn}(t,\vec{p}))_\tau (\overline{\mathcal{N}}(0,\vec{p}))_{\tau'} (\gamma_+)_{\tau'\tau}\rangle \\ &= -f_N \phi^{lmn} \sqrt{Z_N(\vec{p})}\, p_2 p_3 \frac{E(\vec{p})(m_N + E(\vec{p})) + p_1^2}{E(\vec{p})} \\ &\quad \times \exp(-E(\vec{p})t). \end{aligned} \tag{63}$$

C. Next-to-leading twist DAs

For the higher-twist DAs we consider only the operators without derivatives. If we write the operators in Eqs. (27), (28), and (33) with general flavor content,

$$\mathcal{L}_\tau(0) = \epsilon^{abc}[f^{aT}(0) C\gamma_\rho g^b(0)] \times (\gamma_5\gamma_\rho h^c(0))_\tau, \tag{64}$$

$$\mathcal{M}_\tau(0) = \epsilon^{abc}[f^{aT}(0) C\sigma_{\mu\nu} g^b(0)] \times (\gamma_5\sigma_{\mu\nu} h^c(0))_\tau, \tag{65}$$

$$\mathcal{U}_\tau^{L/R}(0) = \epsilon^{abc}[(\gamma_{L/R} g^b)^T(0) C\gamma_{L/R} h^c(0)] \times f_\tau^a(0), \tag{66}$$

we can express them in terms of the irreducible three-quark operators as

$$\mathcal{L} = \sqrt{8} \begin{pmatrix} \mathcal{B}_{3,1}^{lmn} + \mathcal{B}_{4,1}^{lmn} \\ \mathcal{B}_{3,2}^{lmn} + \mathcal{B}_{4,2}^{lmn} \\ \mathcal{B}_{3,3}^{lmn} + \mathcal{B}_{4,3}^{lmn} \\ \mathcal{B}_{3,4}^{lmn} + \mathcal{B}_{4,4}^{lmn} \end{pmatrix}, \qquad \mathcal{M} = \sqrt{96} \begin{pmatrix} \mathcal{B}_{2,1}^{lmn} \\ \mathcal{B}_{2,2}^{lmn} \\ \mathcal{B}_{2,3}^{lmn} \\ \mathcal{B}_{2,4}^{lmn} \end{pmatrix} \tag{67}$$

and

$$\begin{aligned} \gamma_R \mathcal{U}^L - \gamma_L \mathcal{U}^R &= \sqrt{2} \begin{pmatrix} \mathcal{B}_{3,1}^{lmn} \\ \mathcal{B}_{3,2}^{lmn} \\ \mathcal{B}_{3,3}^{lmn} \\ \mathcal{B}_{3,4}^{lmn} \end{pmatrix}, \\ \gamma_L \mathcal{U}^L - \gamma_R \mathcal{U}^R &= \sqrt{2/3} \begin{pmatrix} \mathcal{B}_{1,1}^{lmn} - \mathcal{B}_{2,1}^{lmn} \\ \mathcal{B}_{1,2}^{lmn} - \mathcal{B}_{2,2}^{lmn} \\ \mathcal{B}_{1,3}^{lmn} - \mathcal{B}_{2,3}^{lmn} \\ \mathcal{B}_{1,4}^{lmn} - \mathcal{B}_{2,4}^{lmn} \end{pmatrix}. \end{aligned} \tag{68}$$

After the identification $f \to u$, $g \to u$, and $h \to d$ we restore the proton operators in (27), (28), and (33).

IV. NUMERICAL RESULTS

We have evaluated our correlators on the QCDSF/DIK configurations generated with two flavors of clover fermions at two different β values summarized in Table II. For $\beta = 5.29$ we have used two different lattice sizes, $24^3 \times 48$ and $16^3 \times 32$, each at three different quark masses. For $\beta = 5.40$ we have evaluated the correlators at five different quark masses on $24^3 \times 48$ lattices. The lattice spacing has been set via the Sommer parameter $r_0 = 0.467$ fm [44,45]. As far as possible we have also checked that the dependence of the final results on the fitting procedures discussed below is only very mild and the deviations are consistent with the present statistical errors.

A. General discussion

As already anticipated we can reduce the noise by combining different momenta and/or different operators. However, calculating the general three-quark operator for many momenta turned out to be too expensive. Hence the general correlators (41), and therefore also the correlators for DA operators, were evaluated only for a minimal set of momenta.

To extract the nucleon wave function normalization constant f_N we have fitted the correlator

$$C_0^{000} = \frac{1}{2}(C_{B,0}^{000} + C_{C,0}^{000}), \tag{69}$$

where we have averaged over the two possible correlators at $\vec{p} = \vec{0}$. Similarly, for the first moments we have used

$$C_1^{lmn} = \frac{1}{3}(C_{A,1}^{lmn} + C_{B,1}^{lmn} + C_{C,1}^{lmn}), \tag{70}$$

with $l + m + n = 1$ and $\vec{p} = (2\pi/L, 0, 0)$, where L is the spatial extent of our lattice. For the second moment we have only one correlator, hence no averaging is possible and we have evaluated it for $\vec{p} = (0, 2\pi/L, 2\pi/L)$.

To determine the normalization constant $Z_N(\vec{p})$ we had also to evaluate the usual nucleon correlator. As the additional smearing on the sink introduces additional noise, in particular, for $\vec{p} \neq \vec{0}$, we have improved the signal by using different momenta in the nucleon correlator. For the $16^3 \times 32$ lattices we have worked with

TABLE II. The set of lattices used in our calculation. The scale was set via the Sommer parameter $r_0 = 0.467$ fm.

β	κ	m_π [GeV]	volume	a [fm]	L [fm]
5.29	0.1340, 0.1350, 0.1359	1.411, 1.029, 0.587	$16^3 \times 32$	0.08	1.28
5.29	0.1355, 0.1359, 0.1362	0.800, 0.587, 0.383	$24^3 \times 48$	0.08	1.92
5.40	0.135, 0.1356, 0.1361, 0.13625, 0.1364	1.183, 0.856, 0.648, 0.559, 0.421	$24^3 \times 48$	0.07	1.68

$$C_N^1 = \frac{1}{3}(C_N(2\pi/L,0,0) + C_N(0,2\pi/L,0) + C_N(0,0,2\pi/L)) \quad (71)$$

and

$$C_N^2 = \frac{1}{3}(C_N(0,2\pi/L,2\pi/L) + C_N(2\pi/L,0,2\pi/L) + C_N(2\pi/L,2\pi/L,0)), \quad (72)$$

while for the $24^3 \times 48$ lattices we have used a larger number of momenta:

$$C_N^1 = \frac{1}{3}(C_N(2\pi/L,0,0) + C_N(0,2\pi/L,0) + C_N(0,0,2\pi/L)), \quad (73)$$

$$C_N^2 = \frac{1}{6}(C_N(0,2\pi/L,2\pi/L) + C_N(0,-2\pi/L,2\pi/L) + C_N(2\pi/L,0,2\pi/L) + C_N(2\pi/L,0,-2\pi/L) + C_N(2\pi/L,2\pi/L,0) + C_N(2\pi/L,-2\pi/L,0)). \quad (74)$$

As already mentioned, the location of the effective mass plateaus for the nucleon correlator differs from that for the other correlators as exemplified in Fig. 2. Thus, instead of calculating the ratios of the correlators we have performed a joint fit. As all correlators are evaluated on the same gauge configuration we should also take into account all possible statistical correlations. We have employed two different fitting procedures with different possibilities for incorporating the correlations:

PC: The first possibility is to fit every moment of the DA separately, e.g., for $f_N\phi^{100}$ we fit the correlators C_1^{100} and C_N^1 simultaneously and incorporate the correlations of both correlators and those between different time-slices. However, since we want to extract ϕ^{100} and not $f_N\phi^{100}$ we should in principle also consider the correlation with C^{000}. Because of the omission of these additional correlations we call this procedure ''partially correlated''.

FC: For the second possibility we have estimated the full cross correlation matrix and call this method therefore ''fully correlated''. In this case we fit simultaneously the correlators for the zeroth, first and second moment as well as the nucleon correlator with the same modulus of the momentum.

Both methods have some common disadvantages. In order to extract the moments we have to perform multiparameter fits which involve nucleon mass, different normalization constants and the moments. The second disadvantage is the required knowledge of the smeared-smeared nucleon correlator for nonzero spatial momenta, which introduces additional noise. This requirement can be avoided if we consider ratios of the correlators, which are equal to ratios of moments:

$$l+m+n=1\text{: } R^{lmn} = \frac{\phi^{lmn}}{S_1} = \frac{C_1^{lmn}}{C_{S,1}}, \quad S_1 = \phi^{100} + \phi^{010} + \phi^{001}, \quad C_{S,1} = C_1^{100} + C_1^{010} + C_1^{001}, \quad (75)$$

$$l+m+n=2\text{: } R^{lmn} = \frac{\phi^{lmn}}{S_2} = \frac{C_2^{lmn}}{C_{S,2}}, \quad S_2 = 2(\phi^{011} + \phi^{101} + \phi^{110}) + \phi^{200} + \phi^{020} + \phi^{002}, \quad C_{S,2} = 2(C_2^{011} + C_2^{101} + C_2^{110}) + C_2^{200} + C_2^{020} + C_2^{002}. \quad (76)$$

Now we need additional input to determine the normalization of the moments ϕ^{lmn} with $l+m+n \geq 1$. This can be obtained by using the constraint (25). Thus, we require, e.g., for the first moments that the renormalized moments satisfy

$$\sum_{ij} Z_{ij}\phi_j^{\text{lat}} = 1, \quad (77)$$

where ϕ_i^{lat} are the unrenormalized lattice values

$$\phi_1^{\text{lat}} := \phi^{100}, \qquad \phi_2^{\text{lat}} := \phi^{010}, \qquad \phi_3^{\text{lat}} := \phi^{001} \quad (78)$$

and Z is the renormalization matrix. This leads immediately to a constraint for the ratios $R_i^{\text{lat}} = \phi_i^{\text{lat}}/\sum_j \phi_j^{\text{lat}}$:

$$\sum_i \phi_i^{\text{lat}} = \frac{1}{\sum_{ij} Z_{ij} R_j^{\text{lat}}}. \quad (79)$$

As in this case we use explicitly the constraint (25) we call this analysis method ''constrained''. The calculation of the ratios R^{lmn} does not suffer from the disadvantages mentioned above. Fitting these ratios to a constant we can reach a much higher precision compared to the unconstrained method discussed before. In Fig. 3 we present some of these ratios obtained on one of the ensembles with $\beta = 5.40$. They exhibit longer and less noisy plateaus compared to the correlators in Fig. 2.

The lattice results are obtained at nonphysical quark masses and we have to extrapolate them to the physical point. To our knowledge there are no calculations in chiral

perturbation theory to guide our extrapolation. Therefore we have to rely on the behavior of our data and extrapolate them linearly to the physical point. To estimate the systematic uncertainty of this chiral extrapolation we have performed also an extrapolation including a quadratic term. The systematic uncertainty is then taken to be the difference of the two results.

In the following we present the results of the constrained and unconstrained analysis methods discussed before in the $\overline{\text{MS}}$ scheme at 4 GeV^2 while the raw lattice results are summarized in Appendix C. Using the unconstrained analysis we obtain the normalization constants of the DAs and test how good the constraint in (24) is satisfied. Better results with smaller errors for the higher moments of the leading-twist DA are then obtained from the constrained analysis.

B. Unconstrained analysis

In Table III we present the results for the different constants which are associated with operators without derivatives: the nucleon wave function normalization constant f_N and the next-to-leading twist normalization constants λ_1 and λ_2. Our results confirm the relative signs of f_N, λ_1 and λ_2 calculated in [23,46]. Furthermore we observe $m_N(2\lambda_1 + \lambda_2)/8 = \alpha + \beta \approx 0$ as in [41,47]. This is expected since due to (36) $2\lambda_1 + \lambda_2$ vanishes in the nonrelativistic limit and is known to be small at small quark masses [48].

Our results for the nucleon wave function normalization constant f_N exhibit a clearly nonlinear behavior as a function of m_π^2. However, the dimensionless ratio f_N/m_N^2 is approximately linear [see Fig. 4(a)] and it has the additional advantage that it does not suffer from the uncertainty in setting the scale on the lattice. The chiral behavior of λ_1 and λ_2 is less clear and we have performed two different chiral extrapolations for these quantities. First we have extrapolated the constants λ_i linearly to the physical point and then we have applied the same procedure to the ratios λ_i/m_N. The linear fit looks more favorable for the ratios

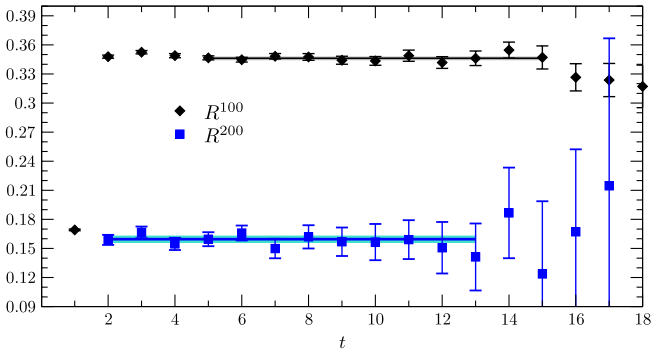

FIG. 3 (color online). Plateaus of correlator ratios R^{100} (black diamonds) and R^{200} (blue squares) for $\beta = 5.40$ and $\kappa = 0.1361$ together with the corresponding fit values and the associated error bands.

λ_i/m_N [see Fig. 4(b)]. Thus we take the results from this fit as our final values, but for comparison we also give the results from the other extrapolation. In contrast to [41,47] we do not observe linear behavior for $m_N\lambda_i$ as a function the quark mass. However, our results from the linear extrapolation of λ_i/m_N are compatible within the errors with those in [41,47].

We have determined the moment combinations $\varphi^{lmn} = 2\phi^{lmn} - \phi^{nml}$ also directly and not from the results for ϕ^{lmn}, using the PC fitting procedure. Thus we had also to compute f_N within this approach. We have also determined λ_i using this analysis method. The results are presented in Table IV. The correlators for higher moments entering the FC fitting procedure seem to favor slightly larger nucleon masses, while the PC analysis leads to somewhat higher values of the normalization constants. We consider the values for the normalization constants obtained within the PC analysis to be more reliable as they are not perturbed by the noisier correlators for the higher moments.

As expected, the nonzero spatial momenta make the results for the first moments noisier than for operators without derivatives. The renormalized results for the moments ϕ^{100}, ϕ^{010}, and ϕ^{001} show clearly the deviation from the asymptotic case with $\phi^{100} = \phi^{010} = \phi^{001} = 1/3$. As the relative differences of these moments describe the deviation from the symmetric case, they are of particular interest in phenomenological applications. Thus we have also determined these differences directly and the bare results from the PC analysis are given in Appendix C. Although these results show a significant deviation from the symmetric case, the errors are large and do not allow reasonable quantitative conclusions. To illustrate these we show in Fig. 5(a) the most important asymmetry $\phi^{100} - \phi^{010}$ normalized by the sum S_1 so that we can compare this later directly with the results from the constrained analysis. However, the results for the moments are less affected by the noise as shown on the example of ϕ^{100} in Fig. 5(b) also normalized by S_1.

We have checked our results by calculating the sums S_1 and S_2 according to Eqs. (75) and (76). The results for the bare and renormalized sums are shown Fig. 6. For the renormalized moments the constraint (24) is fulfilled very well indicating the consistency of our results. Of course the statistical and systematic errors for the case of two derivatives in the operators are higher. Nevertheless, the results still allow us to see the asymmetries. Because of the large errors we give these only for the bare results in Appendix C.

C. Constrained analysis of higher moments

In the last section we have seen that the unconstrained analysis of our data gives us results consistent with theoretical constraint (25). However, better estimates of moments and, in particular, of asymmetries can be obtained from the correlator ratios R^{lmn}. Indeed, the values extracted

TABLE III. Chirally extrapolated results from the FC analysis for normalization constants and the moments ϕ^{lmn} at $\beta = 5.40$ and $\beta = 5.29$ in the $\overline{\text{MS}}$ renormalization scheme at 4 GeV^2. The first error is the combined statistical error of the moments and renormalization matrices. The second (third) errors are the systematic uncertainties due to the chiral extrapolation (renormalization).

β	5.40	5.29
$f_N/m_N^2 \times 10^3$	3.486(60)(56)(60)	3.290(62)(100)(72)
$-\lambda_1/m_N \times 10^3$ [GeV]	40.64(65)(194)(110)	41.24(72)(200)(128)
$-\lambda_1 \times 10^3$ [GeV^2]	49.84(95)(290)(135)	52.47(104)(135)(164)
$\lambda_2/m_N \times 10^3$ [GeV]	80.17(131)(396)(218)	82.08(146)(452)(254)
$\lambda_2 \times 10^3$ [GeV^2]	98.53(189)(601)(268)	105.12(209)(250)(324)
ϕ^{100}	0.3457(75)(89)(3)	0.3530(62)(132)(7)
ϕ^{010}	0.3124(81)(128)(4)	0.3176(62)(108)(2)
ϕ^{001}	0.3142(77)(100)(4)	0.3283(62)(68)(4)
ϕ^{011}	0.0838(73)(266)(44)	0.0851(61)(1)(44)
ϕ^{101}	0.1121(92)(250)(58)	0.1020(66)(179)(68)
ϕ^{110}	0.1051(67)(6)(4)	0.0979(54)(5)(9)
ϕ^{200}	0.1523(106)(699)(129)	0.1639(86)(216)(114)
ϕ^{020}	0.1268(97)(153)(98)	0.1277(79)(1)(76)
ϕ^{002}	0.1398(99)(45)(128)	0.1473(84)(40)(111)

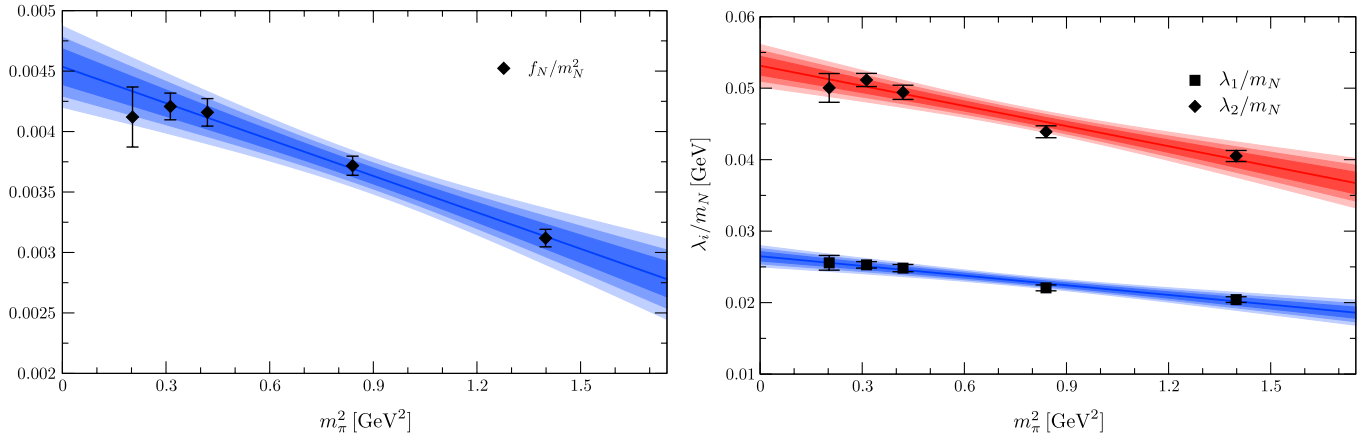

FIG. 4 (color online). Linear chiral extrapolation for f_N/m_N^2 (a) and λ_i/m_N (b) with the 1,2 and 3 sigma error bands.

TABLE IV. Chirally extrapolated PC results for normalization constants and the moments φ^{lmn} at $\beta = 5.40$ and $\beta = 5.29$ in the $\overline{\text{MS}}$ renormalization scheme at 4 GeV^2. The first error is the combined statistical error of the moments and renormalization matrices. The second (third) errors are the systematic uncertainties due to the chiral extrapolation (renormalization). Note that only the values for φ^{lml} can be directly compared with the values for ϕ^{lml} in Table III.

β	5.40	5.29
$f_N/m_N^2 \times 10^3$	3.672(78)(90)(63)	3.538(79)(283)(77)
$-\lambda_1/m_N \times 10^3$ [GeV]	42.19(81)(86)(115)	45.07(92)(315)(140)
$\lambda_2/m_N \times 10^3$ [GeV]	82.91(171)(18)(225)	86.90(87)(641)(261)
φ^{100}	0.3871(313)(528)(4)	0.3903(204)(464)(12)
$\varphi^{010} = \phi^{010}$	0.3150(226)(290)(720)	0.3298(159)(118)(608)
φ^{001}	0.3155(272)(453)(2)	0.3277(190)(270)(5)
φ^{011}	0.0712(180)(127)(92)	0.0827(137)(103)(92)
$\varphi^{101} = \phi^{101}$	0.1091(112)(138)(64)	0.1176(105)(171)(64)
φ^{110}	0.1266(178)(82)(40)	0.1069(137)(103)(49)
φ^{200}	0.1879(250)(942)(135)	0.1709(184)(569)(121)
$\varphi^{020} = \phi^{020}$	0.1275(149)(105)(108)	0.1261(117)(78)(75)
φ^{002}	0.1357(233)(375)(135)	0.1249(193)(296)(109)

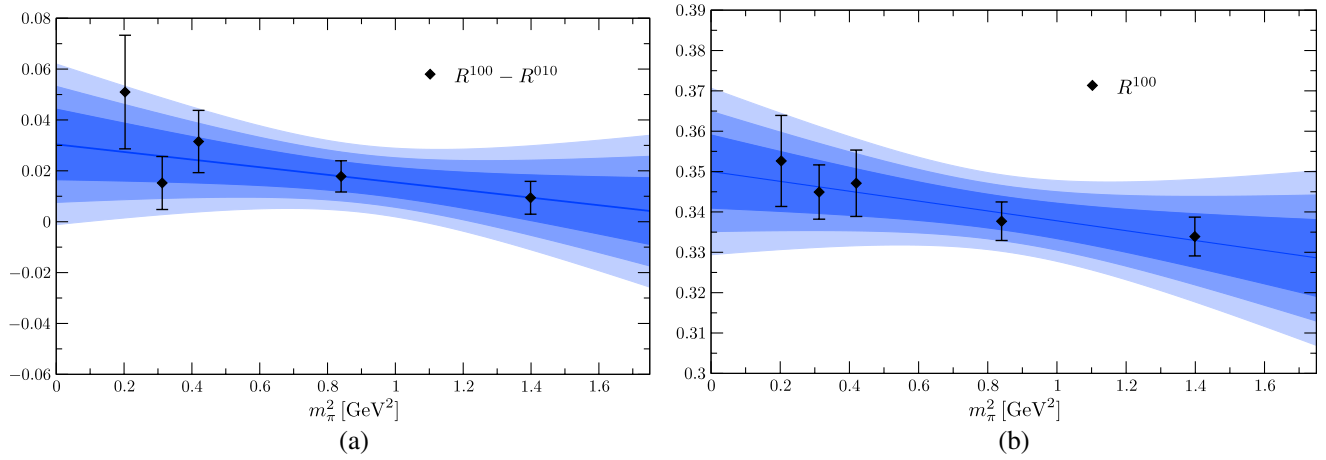

FIG. 5 (color online). Chiral extrapolation of the asymmetry $(\phi^{100} - \phi^{010})/S_1$ (a) from PC results and the ratio ϕ^{100}/S_1 (b) from FC results. We have normalized the values by S_1 so that we are able to compare these directly with the plots in the constrained analysis in Fig. 7.

from the ratios (summarized in Table V) have smaller errors than those from the unconstrained analysis. The main reasons for this improvement are that we do not have to determine the energy $E(\vec{p})$ and normalization constant $Z_N(\vec{p})$ for nonzero spatial momenta as both drop out in the constrained analysis. This reduces also the statistical noise as the nucleon correlator with smeared source and sink is not involved anymore in the data analysis.

The normalization constants f_N and λ_i in Table V were determined by performing a joint fit of all relevant correlators. This approach is equivalent to the FC analysis method. However, as the correlators with higher momenta are not involved the obtained results have smaller errors compared to the FC analysis. Our values for $\alpha = -0.0091 \pm 0.0002_{\rm st} \pm 0.0003_{\rm sys}$ and $\beta = 0.0090 \pm 0.0002_{\rm st} \pm 0.0003_{\rm sys}$ obtained from λ_i/m_N at $\beta = 5.40$ (see Table V) are consistent within the errors with the recent results $\alpha = -0.0112 \pm 0.0012_{\rm st} \pm 0.0022_{\rm sys}$ and $\beta = 0.00120 \pm 0.0013_{\rm st} \pm 0.0023_{\rm sys}$ from simulations with $2 + 1$ flavors of domain-wall fermions [47].

In principle one can calculate similar ratios for correlators involving

$$\varphi^{lmn} = V^{lmn} - A^{lmn}$$

instead of using

$$\phi^{lmn} = (V^{lmn} - A^{lmn} + 2T^{lnm})/3.$$

However, this leads to statistical errors which are about 3 times larger.

To illustrate the dependence of R^{100} on the pion mass we present in Figs. 7(a) and 7(b) linear and quadratic chiral extrapolations of this quantity. As R^{010} exhibits a similar behavior, but with opposite slope, the deviation from a linear dependence is amplified in the asymmetry $R^{100} -$

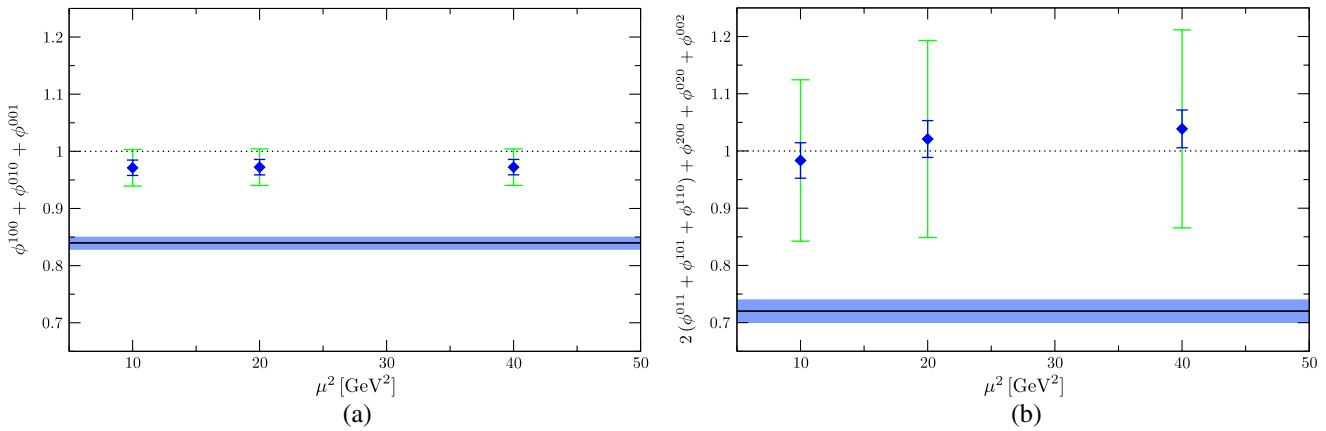

FIG. 6 (color online). The bare (solid black line with statistical error band) and renormalized (blue diamonds) sum of the first moments (a) and second moments (b) according to Eq. (24) as obtained from the FC analysis. The smaller errors for the renormalized values are purely statistical, while the larger ones include the systematical error due to the chiral extrapolation. The three different points were obtained from three different renormalization scales μ in the RI′-MOM scheme to estimate the systematic uncertainty due to the renormalization. The theoretical constraint (25) that the sum should be exactly equal to one is fulfilled in both cases.

TABLE V. The results for ϕ^{lmn} and the relevant asymmetries as obtained from the chirally extrapolated ratios R^{lmn} in the $\overline{\text{MS}}$ renormalization scheme at 4 GeV^2. The values marked by a star were used in the analysis of the corresponding asymmetries to determine the overall normalization. The first error is the combined statistical error of the moments and renormalization matrices dominated by the statistical uncertainties of the moments. The second (third) errors are the systematic uncertainties due to the chiral extrapolation (renormalization).

β	5.40	5.29
$f_N/m_N^2 \times 10^3$	3.573(69)(33)(61)	3.392(68)(178)(74)
$-\lambda_1/m_N \times 10^3$ [GeV]	41.29(74)(45)(113)	42.32(81)(277)(133)
$\lambda_2/m_N \times 10^3$ [GeV]	81.27(149)(90)(221)	83.90(167)(599)(261)
ϕ^{100}	0.3638(11)(68)(3)	0.3549(11)(61)(2)
$\phi^{010} = \varphi^{010}$	0.3023(10)(42)(5)	0.3100(10)(73)(1)
$\phi^{001\star}$	0.3339(9)(26)(2)	0.3351(9)(11)(2)
$\phi^{100} - \phi^{001}$	0.0300(23)(93)(1)	0.0199(23)(46)(4)
$\phi^{001} - \phi^{010}$	0.0313(17)(12)(7)	0.0251(16)(84)(2)
ϕ^{011}	0.0724(18)(82)(70)	0.0863(23)(97)(74)
$\phi^{101} = \varphi^{101}$	0.1136(17)(32)(21)	0.1135(23)(3)(33)
$\phi^{110\star}$	0.0937(16)(3)(38)	0.0953(21)(58)(31)
ϕ^{200}	0.1629(28)(7)(68)	0.1508(38)(213)(64)
$\phi^{020\star} = \varphi^{020}$	0.1289(27)(37)(51)	0.1207(32)(43)(56)
ϕ^{002}	0.1488(32)(77)(73)	0.1385(36)(47)(64)
$\phi^{110} - \phi^{011}$	0.0211(27)(78)(32)	0.0075(33)(69)(44)
$\phi^{101} - \phi^{110}$	0.0204(21)(134)(50)	0.0172(29)(82)(57)
$\phi^{200} - \phi^{020}$	0.0321(33)(69)(55)	0.0335(43)(26)(78)
$\phi^{002} - \phi^{020}$	0.0193(24)(32)(42)	0.0170(36)(8)(56)

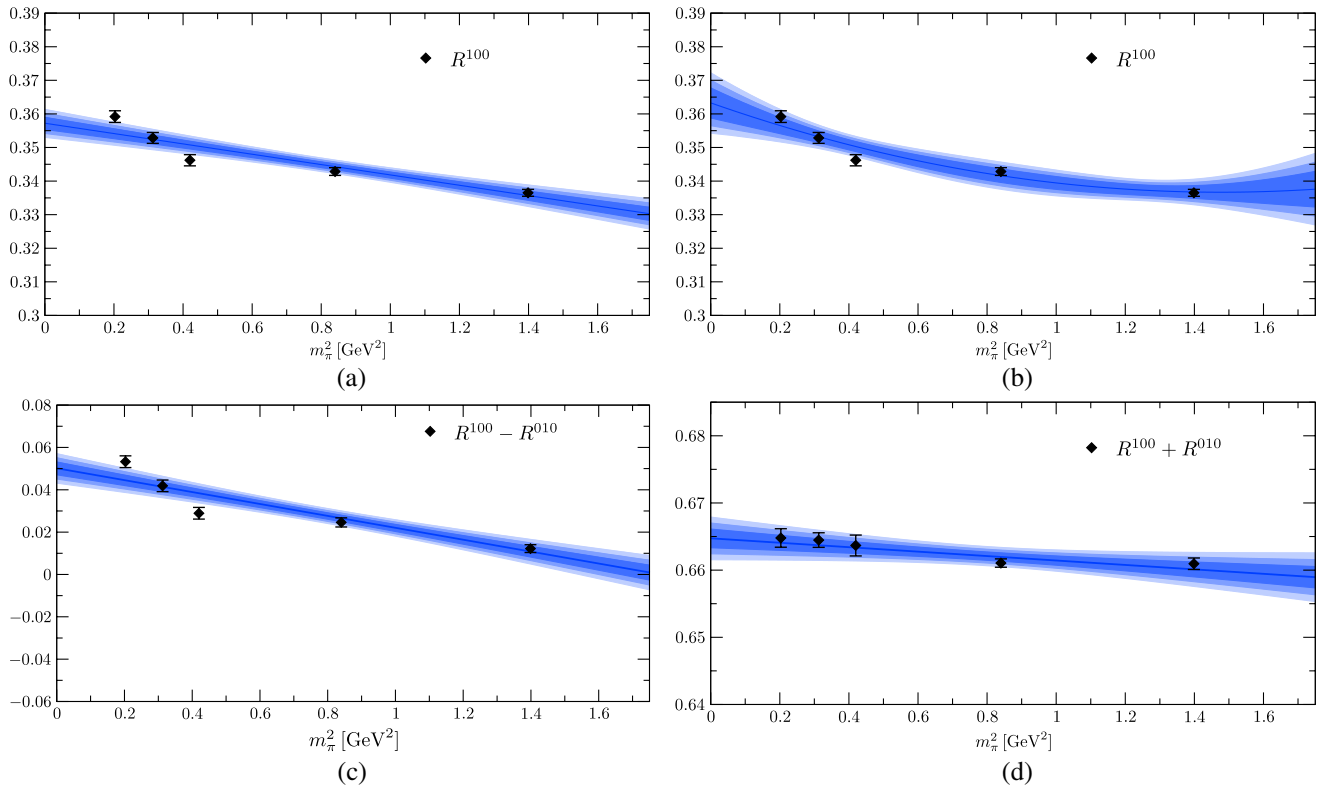

FIG. 7 (color online). The effect of different chiral extrapolations is demonstrated in the case of R^{100} where in (a) a linear fit is performed and in (b) a quadratic one. In the lower plots we show the chiral extrapolation of the asymmetry $R^{100} - R^{010}$ (c) and the sum $R^{100} + R^{010}$ (d). All the plots contain also one, two and three sigma error bands of the corresponding fits.

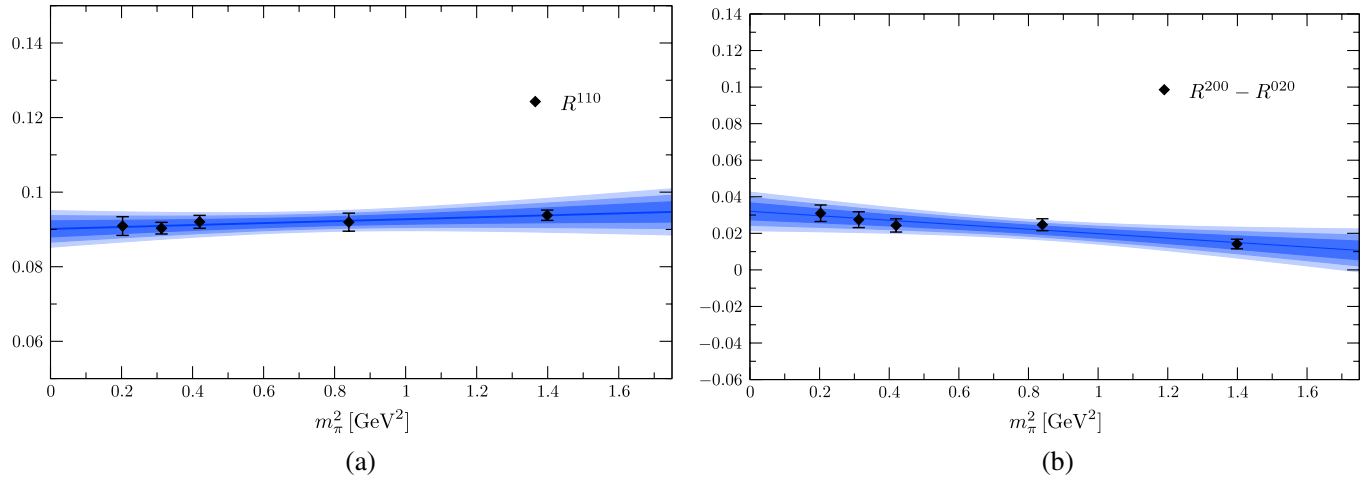

FIG. 8 (color online). Linear chiral extrapolation of the second moment ratio R^{110} (a) and of the asymmetry $R^{200} - R^{020}$ (b) as obtained from the constrained analysis with one, two and three sigma error bands of the corresponding fits.

R^{010} [Fig. 7(c)]. On the other hand, this leads to linear behavior of $R^{100} + R^{010}$ [Fig. 7(d)]. Thus, due to momentum conservation one expects also linear behavior for R^{001}, which is indeed observed in our data. Of course deviations from linear behavior are also possible for all other moments. However, they seem to be smaller than present statistical errors. Comparing the chiral extrapolations in Fig. 5(a) to Fig. 7(c) and in Fig. 5(b) to Fig. 7(a) reveals the increased accuracy of the constrained analysis.

This increase of accuracy is even more important for higher moments. From Figs. 8(a) and 8(b) it is obvious that the improvement for the second moments allows us not only to determine the moments but also the more interesting asymmetries. Even more, with the help of the constraints (24) the moments ϕ^{200}, ϕ^{020}, and ϕ^{002} can be calculated from the other second moments and the first moments. Our results are fully consistent with the direct determination. This approach can be particularly advantageous in the calculation of the third moments as one can then dispense with the evaluation of ϕ^{300}, ϕ^{030}, and ϕ^{003}.

Our data do not allow us to perform a continuum extrapolation. However, the fact that the $\beta = 5.29$ and $\beta = 5.40$ results are compatible with each other indicates that its effect would be small. Thus we take the data from our finer lattice ($\beta = 5.40$) as our final numbers. For convenience we summarize in Table VI the corresponding moments φ^{lmn} at two different renormalization scales as obtained from the $\beta = 5.40$ results in Table V. The change of scales has been performed in the one-loop approximation with $\Lambda_{\overline{\rm MS}} = 226$ MeV. For this purpose the moments ϕ^{lmn}, being not multiplicatively renormalizable, had to be expressed as linear combinations of quantities that are multiplicatively renormalizable, at least in the one-loop approximation, i.e., the coefficients c_{nl} to be introduced in the next section. Their values (and hence also the values of the moments ϕ^{lmn} at the new scale) depend somewhat on the set of moments ϕ^{lmn} that are used as an input. We employed here the set 1 of moments defined in the following section.

TABLE VI. Moments φ^{lmn} as obtained from the independent subset ϕ^{010}, ϕ^{001}, ϕ^{110}, ϕ^{200} and ϕ^{020} at $\beta = 5.40$ in Table V at two different scales $\mu^2 = 4$ GeV^2 and $\mu^2 = 1$ GeV^2 in the $\overline{\rm MS}$ renormalization scheme.

	Asymptotic	$\mu^2 = 4$ GeV^2	$\mu^2 = 1$ GeV^2
$f_N \times 10^3$ [GeV^2]	-	3.144(61)(83)	3.234(63)(86)
$-\lambda_1 \times 10^3$ [GeV^2]	-	38.72(76)(148)	35.57(65)(136)
$\lambda_2 \times 10^3$ [GeV^2]	-	76.23(139)(291)	70.02(128)(268)
φ^{100}	$\frac{1}{3} \approx 0.333$	0.3936(34)(126)	0.3999(37)(139)
φ^{010}	$\frac{1}{3} \approx 0.333$	0.3023(10)(47)	0.2986(11)(52)
φ^{001}	$\frac{1}{3} \approx 0.333$	0.3041(29)(96)	0.3015(32)(106)
φ^{200}	$\frac{1}{7} \approx 0.143$	0.1788(53)(179)	0.1816(64)(212)
φ^{020}	$\frac{1}{7} \approx 0.143$	0.1289(27)(88)	0.1281(32)(106)
φ^{002}	$\frac{1}{7} \approx 0.143$	0.1310(95)(324)	0.1311(113)(382)
φ^{011}	$\frac{2}{21} \approx 0.095$	0.0659(74)(266)	0.0613(89)(319)
φ^{101}	$\frac{2}{21} \approx 0.095$	0.1072(35)(128)	0.1091(41)(152)
φ^{110}	$\frac{2}{21} \approx 0.095$	0.1076(56)(182)	0.1092(67)(219)

V. MODELLING THE NUCLEON DISTRIBUTION AMPLITUDE

Since the available nonperturbative information on the nucleon DA comes in the form of a few first moments, it is tempting to choose a model which is polynomial in momentum fractions at the reference scale μ_0. A natural choice corresponds to the (truncated) expansion in contributions of multiplicatively renormalizable (to leading order) operators of increasing dimension [12,49]:

$$\varphi(x_i,\mu^2) = 120 x_1 x_2 x_3 \sum_{n=0}^{N}\sum_{l=0}^{n} c_{nl} P_{nl}(x_i)\left(\frac{\alpha_s(\mu)}{\alpha_s(\mu_0)}\right)^{\gamma_{nl}/\beta_0}. \tag{80}$$

Here the first subscript, $n = 0,\ldots,N$, is the total number of covariant derivatives in the corresponding operator and simultaneously the order of the polynomial $P_{nl}(x_i)$. The second subscript, $l = 0,\ldots,n$, enumerates independent local operators of the same dimension $D = n + 3$. In this way the scale dependence becomes particularly simple and the functional form is preserved under renormalization in one-loop accuracy. In addition, thanks to the conformal symmetry of the QCD Lagrangian, the polynomials $P_{nl}(x_i)$ are mutually orthogonal with respect to the $SL(2,\mathbb{R})$ scalar product

$$\int [dx] x_1 x_2 x_3 P_{mk}(x_i) P_{nl}(x_i) \propto \delta_{mn}\delta_{kl}. \tag{81}$$

By this reason, the set of moments ϕ^{lmn}, $l + m + n \le 2$, calculated in this work is sufficient to determine uniquely all coefficients in (80) up to $N = 2$, i.e., to second order in the quark momentum fractions. Contributions of higher order polynomials correspond to higher dimension operators and can be added when the corresponding information becomes available.

In the literature there seems to be no standard convention for the normalization of the polynomials $P_{nl}(x_i)$ so we choose the simplest expressions (cf. [12,49]):

$$\begin{aligned}\varphi(x_1,x_2,x_3,\mu^2) = 120 x_1 x_2 x_3 \{ & 1 + c_{10}(\mu_0)(x_1 - 2x_2 + x_3) L^{8/3\beta_0} + c_{11}(\mu_0)(x_1 - x_3) L^{20/9\beta_0} \\ & + c_{20}(\mu_0)[1 + 7(x_2 - 2x_1 x_3 - 2x_2^2)] L^{14/3\beta_0} + c_{21}(\mu_0)(1 - 4x_2)(x_1 - x_3) L^{40/9\beta_0} \\ & + c_{22}(\mu_0)[3 - 9x_2 + 8x_2^2 - 12 x_1 x_3] L^{32/9\beta_0}\},\end{aligned} \tag{82}$$

where

$$L \equiv \frac{\alpha_s(\mu)}{\alpha_s(\mu_0)}, \qquad \beta_0 = 11 - \frac{2}{3} n_F. \tag{83}$$

The scale dependence of the normalization constant is to this accuracy

$$f_N(\mu) = f_N(\mu_0) L^{2/3\beta_0}. \tag{84}$$

The coefficients c_{nl}, $l \le n$, are given in terms of the moments ϕ^{lmn} as

$$c_{10} = \frac{7}{2}(3(\phi^{100} + \phi^{001}) - 2), \tag{85}$$

$$c_{11} = \frac{63}{2}(\phi^{100} - \phi^{001}), \tag{86}$$

$$c_{20} = -\frac{126}{5}(\phi^{200} + \phi^{002} + 3\phi^{101}) + \frac{18}{5}(4 + c_{10}), \tag{87}$$

$$c_{21} = 378(\phi^{200} - \phi^{002}) - 9 c_{11}, \tag{88}$$

$$c_{22} = \frac{126}{5}(2\phi^{200} + 2\phi^{002} + \phi^{101}) - \frac{21}{5}(4 + c_{10}). \tag{89}$$

Note that for $N = 2$ there are five independent coefficients c_{nl}, which is also the number of independent moments ϕ^{lmn} for $l + m + n \le 2$ due to the constraints (24). In the above expressions we have chosen ϕ^{100}, ϕ^{001}, ϕ^{101}, ϕ^{200}, and ϕ^{002} to be the independent subset.

Our final results for the coefficients c_{nl} at the renormalization scale $\mu^2 = 4$ GeV^2 as obtained from the $\beta = 5.40$ moments presented in Table V are collected in Table VII. As the central values for the moments ϕ^{lmn} with $l + m + n = 2$ do not fulfill the constraint (24) exactly, the values of c_{20}, c_{21}, c_{22} depend on the set of moments ϕ^{lmn} that are used as an input. To illustrate this effect, we show two sets of the coefficients obtained from ϕ^{101}, ϕ^{200}, ϕ^{002} (set 1) and ϕ^{101}, ϕ^{011}, ϕ^{110} (set 2). The difference between the two sets is, of course, part of the uncertainty of the calculation. We estimate the overall uncertainty to be about 30% for c_{10}, c_{11}, of order 50% for c_{20}, c_{21} and a factor of 2 for c_{22}.

The resulting shape of the nucleon DA is illustrated in Fig. 9. The asymptotic DA corresponding to the leading term in the expansion (82) is shown in Fig. 9(a). It is totally symmetric in the three quark momentum fractions. The model obtained by adding the terms proportional to c_{10} and c_{11} is presented in Fig. 9(b). Compared to the asymptotic case, the maximum is shifted towards larger values of x_1 indicating that the first quark carries a larger fraction of the proton momentum. Finally, for the plots in Figs. 9(c) and 9(d) we add contributions of the second order polynomials ($n = 2$), using the coefficients c_{20}, c_{21}, c_{22} from the first and the second set in Table VII, respectively. The difference is in fact not too large and the effect is the same in both cases: The maximum is smeared out forming two local maxima and one local minimum. While the model function from set 2 exhibits an approximate symmetry $\varphi(x_1,x_2,x_3) \approx \varphi(x_1,x_3,x_2)$, this property is less obvious in the case of set 1. However, the general pattern is preserved.

Whether the change in the shape of the DA caused by adding the second-order polynomials is of phenomenological significance can only be investigated in a dedicated study, which goes beyond the scope of this work. Note,

TABLE VII. Central values of the coefficients c_{nl} in the expansion (82) at the renormalization scale $\mu^2 = 4$ GeV^2 as obtained from the $\beta = 5.40$ moments presented in Table V.

	Set 1	Set 2
c_{10}	0.326	0.326
c_{11}	0.940	0.940
c_{20}	−0.872	−0.687
c_{21}	−3.130	−5.210
c_{22}	0.405	0.036

however, that in full analogy to usual quantum mechanics, the quality of an approximation to the wave function has to be measured with respect to the scalar product of the appropriate Hilbert space, in our case Eq. (81), and not pointwise in, e.g., the momentum fraction representation.

In Fig. 10 we show $\varphi(x_i)$ at $x_3 = 0.5$ as a function of $x_1(x_2)$ together with the statistical error in order to give an impression of the corresponding uncertainty. The effect of choosing different subsets of ϕ^{lmn} with $l + m + n = 2$ is demonstrated in Fig. 11 where we plot the difference of $\varphi(x_i)$ for set 1 and set 2.

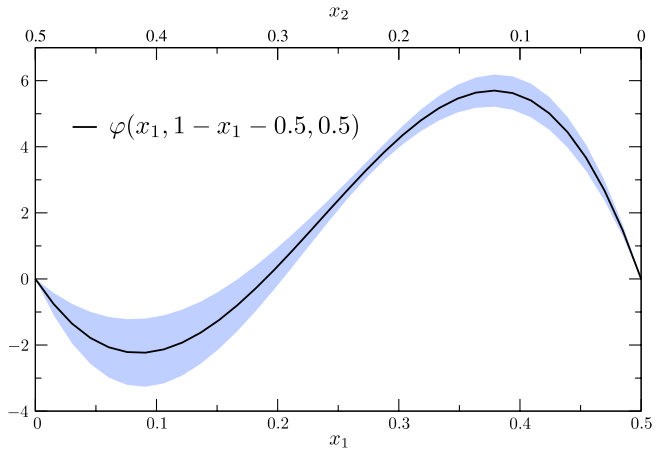

FIG. 10 (color online). The model function $\varphi(x_i)$ at $x_3 = 0.5$ with its statistical uncertainty.

VI. SUMMARY AND CONCLUSIONS

We have evaluated the first few moments of the leading-twist nucleon DA in lattice QCD. Along with these moments we have determined the nucleon couplings to local

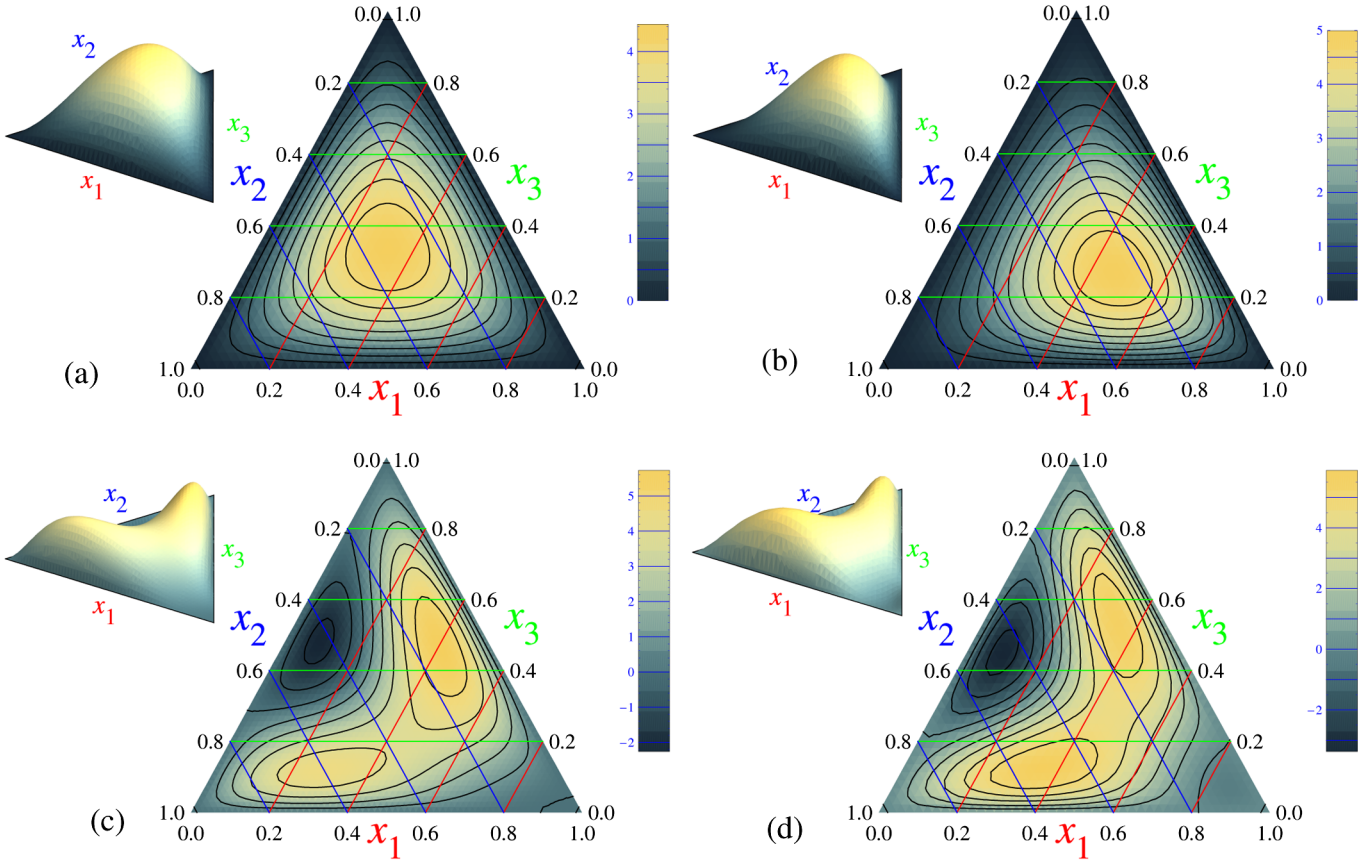

FIG. 9 (color online). Barycentric contour plot of the leading-twist distribution amplitude $\varphi(x_1, x_2, x_3, \mu^2)$ in the limit of $Q^2 = \mu^2 \to \infty$ (a) and at $\mu^2 = 4\text{GeV}^2$ (b–d) using expansion (80) as obtained from the $\beta = 5.40$ moments presented in Table V. The asymmetry caused by the first moments only ($N = 1$) is illustrated in (b), while in (c–d) we took into account also the second moments ($N = 2$). In (c) we have used set 1 and in (d) set 2 as described in the text. The lines of constant x_1, x_2, and x_3 are parallel to the sides of the triangle labeled by x_2, x_3, and x_1, respectively.

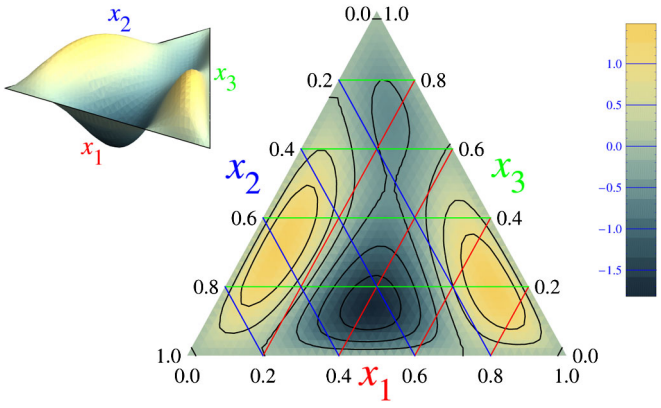

FIG. 11 (color online). Systematic uncertainty due to the choice of the independent subsets of ϕ^{lmn} with $l + m + n = 2$ (for details see text). The lines of constant x_1, x_2, and x_3 are parallel to the sides of the triangle labeled by x_2, x_3, and x_1, respectively.

subleading (twist-four) operators. The required correlators have been computed on gauge field configurations generated by the QCDSF/DIK collaborations using two dynamical flavors of clover fermions. The necessary renormalization matrices have been calculated nonperturbatively, including the mixing with operators containing total derivatives.

We have worked with two different gauge couplings corresponding to $\beta = 5.29$ and $\beta = 5.40$. For the lattice sizes and quark masses see Table II. As our final numbers we take the data from our finer lattice ($\beta = 5.40$). The results for the moments of the leading-twist DA at two different renormalization scales are presented in Table VI. The corresponding coefficients in the expansion of the DA in a basis of orthogonal polynomials are given in Table VII. Truncating this expansion at the second order, we obtain a model of the DA which is plotted in Fig. 9. Our error estimates include statistic and known sources of systematic uncertainties, but still have to be considered with some caution. The largest uncertainty is caused by the chiral extrapolation. We expect that it will be reduced in the relatively near future when simulations with smaller pion masses on larger lattices become available.

Our value for the coupling f_N, which determines the normalization of the leading-twist nucleon DA, appears to be approximately 40% below the corresponding QCD sum rule estimates [8,9,19]. If confirmed, this result would deal yet another blow at the hopes to calculate the nucleon magnetic form factor at realistic momentum transfers within perturbative QCD. At the same time, the twist-four couplings λ_1 and λ_2, which are related to the normalization of subleading twist-four DAs, turn out to be in agreement with other estimates. These constants are relevant, e.g., for the description of form factors involving a helicity flip within perturbative QCD [24] and also for soft (end point) corrections to the form factors in the light-cone sum rule approach [25,50]. The same constants enter the effective baryon chiral Lagrangian and can be used to estimate the proton life time within GUT models.

The results we have obtained for the first moments of the nucleon DA are consistent with the conventional picture that the valence u-quark with helicity parallel to that of the proton carries the largest fraction of its momentum, but the effect seems to be less pronounced compared to the corresponding QCD sum rule calculations [8,9,19]. Our numbers, however, are compatible with those extracted from the fits to the electromagnetic proton form factors within the light-cone sum rule approach [50].

Our calculation of the second moments of the DA indicates the presence of considerable second-order contributions in the expansion in terms of orthogonal polynomials. Qualitatively, these contributions smear out the maximum forming two local maxima and one local minimum [see Figs. 9(c) and 9(d)]. The investigation of the phenomenological consequences of these and other features of our model DA, such as the approximate symmetry $\varphi(x_1, x_2, x_3) \approx \varphi(x_1, x_3, x_2)$, requires a dedicated study, which goes beyond the scope of the present work and will be presented elsewhere.

ACKNOWLEDGMENTS

We are grateful to A. Lenz, J. Bloch and A. Manashov for helpful discussions. The numerical calculations have been performed on the Hitachi SR8000 at LRZ (Munich), apeNEXT and APEmille at NIC/DESY (Zeuthen) and BlueGene/Ls at NIC/JSC (Jülich), EPCC (Edinburgh), and KEK (by the Kanazawa group as part of the DIK research program) as well as QCDOC (Regensburg) using the Chroma software library [51,52]. This work was supported by DFG (Forschergruppe Gitter-Hadronen-Phänomenologie and SFB/TR55 Hadron Physics from Lattice QCD), by EU I3HP (Contract No. RII3-CT-2004-506078) and by BMBF.

APPENDIX A: DIRAC MATRICES IN WEYL REPRESENTATION

We have used the following representation of the Euclidean Dirac matrices:

$$\gamma_1 = \begin{pmatrix} 0 & 0 & 0 & i \\ 0 & 0 & i & 0 \\ 0 & -i & 0 & 0 \\ -i & 0 & 0 & 0 \end{pmatrix}, \quad \gamma_2 = \begin{pmatrix} 0 & 0 & 0 & 1 \\ 0 & 0 & -1 & 0 \\ 0 & -1 & 0 & 0 \\ 1 & 0 & 0 & 0 \end{pmatrix},$$
$$\gamma_3 = \begin{pmatrix} 0 & 0 & i & 0 \\ 0 & 0 & 0 & -i \\ -i & 0 & 0 & 0 \\ 0 & i & 0 & 0 \end{pmatrix}, \quad \gamma_4 = \begin{pmatrix} 0 & 0 & 1 & 0 \\ 0 & 0 & 0 & 1 \\ 1 & 0 & 0 & 0 \\ 0 & 1 & 0 & 0 \end{pmatrix} \quad \text{(A1)}$$

with

$$\gamma_5 = \gamma_1\gamma_2\gamma_3\gamma_4 = \begin{pmatrix} -1 & 0 & 0 & 0 \\ 0 & -1 & 0 & 0 \\ 0 & 0 & 1 & 0 \\ 0 & 0 & 0 & 1 \end{pmatrix}, \qquad \sigma_{\mu\nu} = \frac{i}{2}(\gamma_\mu\gamma_\nu - \gamma_\nu\gamma_\mu). \tag{A2}$$

The charge conjugation matrix has been chosen as

$$C = \gamma_2\gamma_4. \tag{A3}$$

APPENDIX B: OPERATOR RELATIONS FOR LEADING-TWIST DISTRIBUTION AMPLITUDES

In the following we give the relations between the operators whose matrix elements define moments of the leading-twist DA of spin-1/2 baryons (DA operators) and the irreducible operators that appear in the general group-theoretical classification in [31]. The relations are written for general quark flavors f, g, h; the proton case is obtained by the replacement f, $g \to u$, $h \to d$, and the appropriate symmetrization to single out the contribution of isospin 1/2.

The total symmetrization in space-time indices denoted by the curly brackets, e.g.,

$$\mathcal{V}^{\{23\}} = \frac{1}{2!}(\mathcal{V}^{23} + \mathcal{V}^{32})$$

reflects the leading-twist projection. For example, the moment V^{001} is calculated from

$$\frac{1}{2!}\epsilon^{abc}([f(0)]^a_\alpha(C\gamma_2)_{\alpha\beta}[g(0)]^b_\beta[iD_3(\gamma_5 h(0))]^c_\tau + [f(0)]^a_\alpha(C\gamma_3)_{\alpha\beta}[g(0)]^b_\beta[iD_2(\gamma_5 h(0))]^c_\tau). \tag{B1}$$

In the notation used below, it is not indicated explicitly on which quark the derivatives act in the operators on the right-hand side. However, it is always implied that the positions of the derivatives are the same on both sides of the equations.

1. 0th moment

$$(\mathcal{B}^{000}_{9,6}, -\mathcal{B}^{000}_{9,1}, -\mathcal{B}^{000}_{9,12}, \mathcal{B}^{000}_{9,7}) = \frac{1}{4}(\gamma_3\gamma_4[\gamma_2\mathcal{T}^1 + \gamma_1\mathcal{T}^2]), \tag{B2}$$

$$(\mathcal{B}^{000}_{9,4}, -\mathcal{B}^{000}_{9,3}, -\mathcal{B}^{000}_{9,10}, \mathcal{B}^{000}_{9,9}) = \frac{1}{4}(\gamma_1\gamma_2[\gamma_4\mathcal{T}^3 + \gamma_3\mathcal{T}^4]), \tag{B3}$$

$$(\mathcal{B}^{000}_{9,2}, -\mathcal{B}^{000}_{9,5}, -\mathcal{B}^{000}_{9,8}, \mathcal{B}^{000}_{9,11}) = \frac{1}{4\sqrt{2}}(\gamma_1\gamma_2[\gamma_4\mathcal{T}^3 - \gamma_3\mathcal{T}^4] + \gamma_3\gamma_4[\gamma_1\mathcal{T}^2 - \gamma_2\mathcal{T}^1]). \tag{B4}$$

The $\mathcal{B}^{000}_{7,i}$ ($\mathcal{B}^{000}_{8,i}$) operators from the symmetry class $-++$ ($+-+$) are obtained from the above operators by replacing $\mathcal{T}$ on the right-hand side by $\mathcal{V} + \mathcal{A}$ ($\mathcal{V} - \mathcal{A}$).

2. 1st moments

$$(\mathcal{B}^{lmn}_{7,1}, -\mathcal{B}^{lmn}_{7,2}, \mathcal{B}^{lmn}_{7,7}, -\mathcal{B}^{lmn}_{7,8}) = \frac{1}{4\sqrt{2}}(2\gamma_4\gamma_3\mathcal{T}^{\{12\}} + \gamma_4\gamma_2\mathcal{T}^{\{13\}} + \gamma_2\gamma_3\mathcal{T}^{\{14\}} + \gamma_4\gamma_1\mathcal{T}^{\{23\}} + \gamma_1\gamma_3\mathcal{T}^{\{24\}}), \tag{B5}$$

$$(\mathcal{B}^{lmn}_{7,3}, -\mathcal{B}^{lmn}_{7,4}, \mathcal{B}^{lmn}_{7,9}, -\mathcal{B}^{lmn}_{7,10}) = \frac{1}{4\sqrt{2}}(2\gamma_1\gamma_2\mathcal{T}^{\{34\}} + \gamma_4\gamma_2\mathcal{T}^{\{13\}} + \gamma_3\gamma_2\mathcal{T}^{\{14\}} + \gamma_1\gamma_4\mathcal{T}^{\{23\}} + \gamma_1\gamma_3\mathcal{T}^{\{24\}}), \tag{B6}$$

$$(\mathcal{B}^{lmn}_{7,6}, \mathcal{B}^{lmn}_{7,5}, \mathcal{B}^{lmn}_{7,12}, \mathcal{B}^{lmn}_{7,11}) = \frac{1}{4}(\gamma_2\gamma_4\mathcal{T}^{\{13\}} + \gamma_2\gamma_3\mathcal{T}^{\{14\}} + \gamma_1\gamma_4\mathcal{T}^{\{23\}} + \gamma_1\gamma_3\mathcal{T}^{\{24\}}). \tag{B7}$$

The $\mathcal{B}^{lmn}_{5,i}$ ($\mathcal{B}^{lmn}_{6,i}$) operators from the symmetry class $D-++$ ($D+-+$) are obtained from the above operators by replacing $\mathcal{T}$ on the right-hand side by $\mathcal{V} + \mathcal{A}$ ($\mathcal{V} - \mathcal{A}$).

3. 2nd moments

$$(-\mathcal{B}^{lmn}_{6,4}, -\mathcal{B}^{lmn}_{6,3}, \mathcal{B}^{lmn}_{6,2}, \mathcal{B}^{lmn}_{6,1}) = \frac{\sqrt{3}}{4}(\gamma_4\mathcal{T}^{\{123\}} + \gamma_3\mathcal{T}^{\{124\}} + \gamma_2\mathcal{T}^{\{134\}} + \gamma_1\mathcal{T}^{\{234\}}) \tag{B8}$$

The $\mathcal{B}^{lmn}_{4,i}$ ($\mathcal{B}^{lmn}_{5,i}$) operators from the symmetry class $DD-++$ ($DD+-+$) are obtained from the above operators by replacing $\mathcal{T}$ on the right-hand side by $\mathcal{V} + \mathcal{A}$ ($\mathcal{V} - \mathcal{A}$).

APPENDIX C: RAW LATTICE RESULTS

In this appendix we collect the results of the linear (in m_π^2) extrapolation of our bare lattice data. The errors given are purely statistical.

TABLE VIII. Linear extrapolations of FC (unconstrained) results to the physical point using all available lattice ensembles (all) and $24^3 \times 48$ lattices only (24) for $\beta = 5.29$. The χ^2/d.o.f refers to the linear chiral extrapolation.

	$\beta = 5.29$				$\beta = 5.40$	
	all		24		all	
	#	χ^2/d.o.f	#	χ^2/d.o.f	#	χ^2/d.o.f
$f_N/m_N^2 \times 10^3$	4.088(77)	6.563	4.53(14)	0.555	4.287(74)	0.658
$-\lambda_1/m_N \times 10^3$ [GeV]	60.80(106)	19.31	69.28(176)	6.209	59.40(95)	1.060
$-\lambda_1 \times 10^3$ [GeV^2]	77.33(149)	18.46	82.24(209)	3.484	72.86(135)	1.901
$\lambda_2/m_N \times 10^3$ [GeV]	129.76(214)	19.98	141.53(360)	4.928	119.16(191)	1.498
$\lambda_2 \times 10^3$ [GeV^2]	158.00(315)	18.31	168.30(428)	2.388	146.48(270)	2.716
ϕ^{100}	0.2987(49)	1.125	0.315(10)	0.033	0.2939(59)	1.384
ϕ^{010}	0.2746(48)	0.768	0.263(11)	0.765	0.2719(62)	0.335
ϕ^{001}	0.2840(48)	1.566	0.271(11)	2.555	0.2740(60)	0.972
ϕ^{011}	0.0647(37)	0.276	0.0633(87)	0.711	0.0646(44)	1.831
ϕ^{101}	0.0606(39)	0.821	0.067(12)	0.744	0.0688(55)	1.057
ϕ^{110}	0.0651(32)	0.712	0.0592(79)	0.445	0.0707(39)	0.610
ϕ^{200}	0.1149(54)	2.367	0.146(14)	0.597	0.1126(68)	5.534
ϕ^{020}	0.0922(50)	0.717	0.096(12)	1.908	0.0949(61)	0.288
ϕ^{002}	0.1067(54)	0.944	0.108(13)	2.729	0.1060(64)	0.114

TABLE IX. Linear extrapolations of PC (unconstrained) results to the physical point using all available lattice ensembles (all) and $24^3 \times 48$ lattices only (24) for $\beta = 5.29$. The χ^2/d.o.f refers to the linear chiral extrapolation.

	$\beta = 5.29$				$\beta = 5.40$	
	all		24		all	
	#	χ^2/d.o.f	#	χ^2/d.o.f	#	χ^2/d.o.f
$f_N/m_N^2 \times 10^3$	4.396(99)	2.417	4.67(19)	1.208	4.517(96)	0.342
$V^{100} = V^{010}$	0.308(13)	0.416	0.298(35)	0.027	0.298(19)	0.966
$A^{100} = -A^{010}$	0.0133(40)	2.495	0.046(13)	0.038	0.0196(64)	0.960
$T^{100} = T^{010}$	0.307(12)	0.425	0.297(25)	0.263	0.300(16)	0.483
φ^{100}	0.324(16)	0.352	0.360(49)	0.001	0.323(24)	0.777
$\varphi^{010} = \phi^{010} = T^{001}$	0.286(12)	1.636	0.248(26)	0.550	0.276(17)	0.446
$\varphi^{001} = V^{001}$	0.289(15)	1.892	0.229(37)	1.532	0.280(21)	0.399
$\phi^{100} - \phi^{010}$	0.0194(49)	2.230	0.054(15)	0.056	0.0258(77)	0.928
$\phi^{100} - \phi^{001}$	0.0076(39)	2.017	0.036(14)	1.011	0.0129(66)	1.291
$\phi^{001} - \phi^{010}$	0.0114(41)	0.679	0.016(13)	1.719	0.0144(66)	2.118
$V^{011} = V^{101}$	0.0698(56)	0.197	0.072(17)	0.228	0.0676(69)	0.260
$A^{011} = -A^{101}$	−0.0006(49)	0.038	0.000(15)	0.004	0.0022(60)	1.063
$T^{011} = T^{101}$	0.0689(44)	0.395	0.068(12)	0.035	0.0707(54)	0.580
φ^{011}	0.0709(85)	0.068	0.076(27)	0.061	0.064(11)	0.533
$\varphi^{101} = \phi^{101} = T^{110}$	0.0699(62)	0.428	0.071(18)	0.135	0.0673(67)	0.504
$\varphi^{110} = V^{110}$	0.0637(79)	0.149	0.064(24)	0.101	0.077(10)	0.049
$\phi^{101} - \phi^{011}$	0.0012(62)	0.068	0.006(19)	0.023	0.0005(73)	1.711
$\phi^{011} - \phi^{110}$	0.0025(45)	0.048	0.004(15)	0.096	−0.0042(62)	0.246
$\phi^{101} - \phi^{110}$	−0.0001(47)	0.155	0.005(17)	0.383	−0.0036(62)	0.627
$V^{200} = V^{020}$	0.1059(78)	0.557	0.129(22)	0.015	0.115(10)	2.034
$A^{020} = -A^{200}$	0.0132(59)	0.698	0.036(18)	0.131	0.0195(81)	1.812
$T^{200} = T^{020}$	0.1108(79)	0.576	0.119(19)	1.336	0.1203(89)	1.450
φ^{200}	0.117(12)	0.739	0.165(37)	0.006	0.134(16)	2.305
$\varphi^{020} = \phi^{020} = T^{002}$	0.0913(73)	0.261	0.097(19)	0.590	0.0963(93)	0.646
$\varphi^{002} = V^{002}$	0.096(12)	0.724	0.066(35)	1.320	0.106(15)	0.279
$\phi^{200} - \phi^{020}$	0.0206(68)	0.406	0.039(21)	0.001	0.0300(97)	1.864
$\phi^{200} - \phi^{002}$	0.0060(61)	0.847	0.032(20)	0.601	0.0092(83)	1.380
$\phi^{002} - \phi^{020}$	0.0114(55)	0.291	0.005(19)	0.757	0.0215(80)	0.438

TABLE X. Linear extrapolations of ϕ^{lmn} and asymmetries to the physical point as obtained from the constrained analysis using all available ensembles. The χ^2/d.o.f refers to the linear chiral extrapolation. The values denoted by the $\star$ were used to determine the absolute normalization of the associated asymmetries.

	$\beta = 5.29$		$\beta = 5.40$	
	#	χ^2/d.o.f	#	χ^2/d.o.f
$f_N/m_N^2 \times 10^3$	4.215(85)	1.878	4.395(85)	0.267
$-\lambda_1/m_N \times 10^3$ [GeV]	51.10(117)	10.57	60.35(108)	0.184
$\lambda_2/m_N \times 10^3$ [GeV]	125.75(25)	10.54	120.80(216)	0.403
ϕ^{100}	0.3286(12)	7.559	0.3358(11)	6.115
$\phi^{010} = \varphi^{010}$	0.2943(9)	8.530	0.2891(9)	6.960
$\phi^{001}(\star)$	0.3164(9)	1.112	0.3155(9)	1.312
$\phi^{100} - \phi^{010}$	0.0350(20)	9.960	0.0468(19)	7.732
$\phi^{100} - \phi^{001}$	0.0126(19)	3.996	0.0206(18)	3.300
$\phi^{001} - \phi^{010}$	0.0225(14)	3.315	0.0263(14)	2.526
ϕ^{011}	0.1113(26)	3.593	0.0932(19)	1.544
ϕ^{101}	0.1148(26)	0.370	0.1124(18)	0.287
$\phi^{110}(\star)$	0.1085(22)	1.716	0.1034(16)	0.135
ϕ^{200}	0.1820(44)	4.176	0.1924(30)	0.338
$\phi^{020} = \varphi^{020}(\star)$	0.1489(35)	0.363	0.1539(28)	0.265
ϕ^{002}	0.1728(42)	1.677	0.1801(36)	0.856
$\phi^{101} - \phi^{011}$	0.0042(39)	2.489	0.0200(27)	0.900
$\phi^{110} - \phi^{011}$	0.0042(34)	0.636	0.0100(25)	0.775
$\phi^{101} - \phi^{110}$	0.0053(29)	1.159	0.0094(20)	0.257
$\phi^{200} - \phi^{020}$	0.0367(48)	1.515	0.0364(35)	0.514
$\phi^{200} - \phi^{002}$	0.0076(59)	1.763	0.0115(39)	0.810
$\phi^{002} - \phi^{020}$	0.0230(39)	1.010	0.0255(24)	0.597

[1] G. P. Lepage and S. J. Brodsky, Phys. Rev. Lett. **43**, 545 (1979); **43**, 1625(E) (1979).
[2] S. J. Brodsky, G. P. Lepage, and S. A. A. Zaidi, Phys. Rev. D **23**, 1152 (1981).
[3] S. J. Brodsky and G. P. Lepage, Phys. Rev. D **24**, 2848 (1981).
[4] V. L. Chernyak, A. R. Zhitnitsky, and V. G. Serbo, JETP Lett. **26**, 594 (1977).
[5] A. V. Efremov and A. V. Radyushkin, Phys. Lett. B **94**, 245 (1980).
[6] G. P. Lepage and S. J. Brodsky, Phys. Lett. B **87**, 359 (1979).
[7] G. P. Lepage and S. J. Brodsky, Phys. Rev. D **22**, 2157 (1980).
[8] V. L. Chernyak and I. R. Zhitnitsky, Nucl. Phys. **B246**, 52 (1984).
[9] V. L. Chernyak, A. A. Ogloblin, and I. R. Zhitnitsky, Z. Phys. C **42**, 569 (1989).
[10] M. E. Peskin, Phys. Lett. B **88**, 128 (1979).
[11] S. J. Brodsky, Y. Frishman, G. P. Lepage, and C. T. Sachrajda, Phys. Lett. B **91**, 239 (1980).
[12] V. M. Braun, S. E. Derkachov, G. P. Korchemsky, and A. N. Manashov, Nucl. Phys. **B553**, 355 (1999).
[13] V. M. Braun, A. N. Manashov, and J. Rohrwild, Nucl. Phys. **B807**, 89 (2009).
[14] V. M. Braun, S. E. Derkachov, and A. N. Manashov, Phys. Rev. Lett. **81**, 2020 (1998).
[15] M. K. Jones *et al.* (Jefferson Lab Hall A Collaboration), Phys. Rev. Lett. **84**, 1398 (2000).
[16] O. Gayou *et al.*, Phys. Rev. C **64**, 038202 (2001).
[17] O. Gayou *et al.* (Jefferson Lab Hall A Collaboration), Phys. Rev. Lett. **88**, 092301 (2002).
[18] V. Punjabi *et al.*, Phys. Rev. C **71**, 055202 (2005); **71**, 069902(E) (2005).
[19] I. D. King and C. T. Sachrajda, Nucl. Phys. **B279**, 785 (1987).
[20] K. C. Bowler *et al.*, Nucl. Phys. **B296**, 431 (1988).
[21] G. Martinelli and C. T. Sachrajda, Phys. Lett. B **217**, 319 (1989).
[22] M. B. Gavela *et al.*, Nucl. Phys. **B312**, 269 (1989).
[23] V. Braun, R. J. Fries, N. Mahnke, and E. Stein, Nucl. Phys. **B589**, 381 (2000); **B607**, 433(E) (2001).
[24] A. V. Belitsky, X. Ji, and F. Yuan, Phys. Rev. Lett. **91**, 092003 (2003).
[25] V. M. Braun, A. Lenz, N. Mahnke, and E. Stein, Phys. Rev. D **65**, 074011 (2002).
[26] A. Lenz, M. Wittmann, and E. Stein, Phys. Lett. B **581**, 199 (2004).
[27] M. Göckeler *et al.*, Phys. Rev. Lett. **101**, 112002 (2008).
[28] N. Warkentin *et al.*, arXiv:0811.2212.
[29] M. Göckeler *et al.*, Phys. Rev. D **54**, 5705 (1996).
[30] M. Göckeler *et al.* (QCDSF Collaboration), Proc. Sci., LAT2007 (2007) 147.
[31] T. Kaltenbrunner, M. Göckeler, and A. Schäfer, Eur. Phys. J. C **55**, 387 (2008).
[32] A. B. Henriques, B. H. Kellett, and R. G. Moorhouse, Ann.

Phys. (N.Y.) **93**, 125 (1975).
[33] V. L. Chernyak and A. R. Zhitnitsky, Phys. Rep. **112**, 173 (1984).
[34] B. L. Ioffe, Nucl. Phys. **B188**, 317 (1981); **B191**, 591(E) (1981).
[35] Y. Chung, H. G. Dosch, M. Kremer, and D. Schall, Nucl. Phys. **B197**, 55 (1982).
[36] Y. Tomozawa, Phys. Rev. Lett. **46**, 463 (1981); **49**, 507(E) (1982).
[37] M. B. Wise, R. Blankenbecler, and L. F. Abbott, Phys. Rev. D **23**, 1591 (1981).
[38] M. Claudson, M. B. Wise, and L. J. Hall, Nucl. Phys. **B195**, 297 (1982).
[39] V. S. Berezinsky, B. L. Ioffe, and Y. I. Kogan, Phys. Lett. B **105**, 33 (1981).
[40] S. J. Brodsky, J. R. Ellis, J. S. Hagelin, and C. T. Sachrajda, Nucl. Phys. **B238**, 561 (1984).
[41] Y. Aoki, C. Dawson, J. Noaki, and A. Soni, Phys. Rev. D **75**, 014507 (2007).
[42] M. Göckeler *et al.*, (QCDSF/UKQCD Collaborations), Nucl. Phys. **B812**, 205 (2009).
[43] T. Kaltenbrunner, PhD thesis, University of Regensburg, 2008.
[44] A. Ali Khan *et al.*, Phys. Rev. D **74**, 094508 (2006).
[45] C. Aubin *et al.*, Phys. Rev. D **70**, 094505 (2004).
[46] A. V. Kolesnichenko, Sov. J. Nucl. Phys. **39**, 968 (1984).
[47] Y. Aoki *et al.*, (RBC-UKQCD Collaboration), Phys. Rev. D **78**, 054505 (2008).
[48] S. Sasaki, T. Blum, and S. Ohta, Phys. Rev. D **65**, 074503 (2002).
[49] N. G. Stefanis, Eur. Phys. J. direct C **7**, 1 (1999).
[50] V. M. Braun, A. Lenz, and M. Wittmann, Phys. Rev. D **73**, 094019 (2006).
[51] R. G. Edwards and B. Joó (SciDAC Collaboration and LHPC Collaboration and UKQCD Collaboration), Nucl. Phys. B, Proc. Suppl. **140**, 832 (2005).
[52] P. A. Boyle, http://www.ph.ed.ac.uk/~paboyle/bagel/Bagel.html (2005).